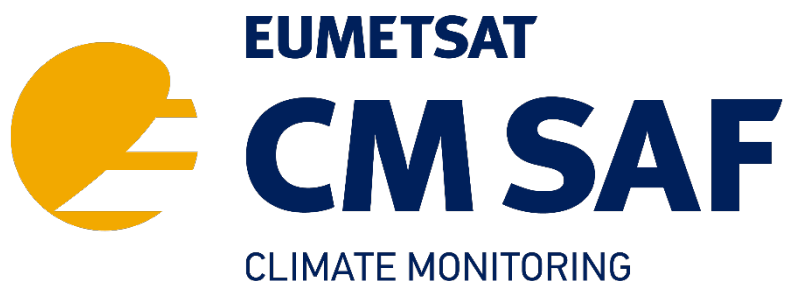


EUMETSAT Satellite Application Facility on Climate Monitoring



Algorithm Theoretical Baseline Document

**Meteosat Solar Surface Radiation and effective Cloud
Albedo Climate Data Records - Heliosat**

SARAH-3


**The MAGIC SOL method applied for the generation of
SARAH-3**

DOI: 10.5676/EUM_SAF_CM/SARAH/V003

	CDR	ICDR
Effective Cloud Albedo (CAL)	CM-23083	CM-5081
Surface Incoming Shortwave Radiation (SIS):	CM-23203	CM-5211
Surface Direct Irradiance (SDI):	CM-23293	CM-5291
Sunshine Duration (SDU):	CM-23283	CM-5281
Photosynthetic Active Radiation (PAR):	CM-23273	CM-5271
Daylight (DAL):	CM-23253	CM-5251

Reference Number:
Issue/Revision Index:
Date:

SAF/CM/DWD/ATBD/SARAH
3.5
24.02.2023

	Algorithm Theoretical Basis Document SARAH-3	Doc. No: SAF/CM/DWD/ATBD/SARAH Issue: 3.5 Date: 24.02.2023
---	---	--

Document Signature Table

	Name	Function	Signature	Date
Author	Uwe Pfeifroth Jörg Trentmann	CM SAF scientists		24/02/2023
Review	Marc Schröder	CM SAF Science Coordinator		01/03/2023
Approval	CM SAF Steering Group			
Release	Rainer Hollmann	Project Manager		


Distribution List

Internal Distribution	
Name	No. Copies
DWD Archive	1
CM SAF Team	1

External Distribution		
Company	Name	No. Copies
PUBLIC		1

Document Change Record

Issue/ Revision	Date	DCN No.	Changed Pages/Paragraphs
1.0	01/09/2013	SAF/CM/DWD/ATBD/METEOSAT/HEL	First official version.
1.1	02/12/2013	SAF/CM/DWD/ATBD/METEOSAT/HEL	Review Comments included
1.2	08/08/2014	SAF/CM/DWD/ATBD/METEOSAT/HEL	Added/modified paragraph 4.4 about the used aerosol

	Algorithm Theoretical Basis Document SARAH-3	Doc. No: SAF/CM/DWD/ATBD/SARAH Issue: 3.5 Date: 24.02.2023
---	---	--

Issue/ Revision	Date	DCN No.	Changed Pages/Paragraphs
			information
1.3	01/11/2014	SAF/CM/DWD/ATBD/METEOSAT/HEL	Modifications according DRR2.1 review comments.
2.0	14/08/2015	SAF/CM/DWD/ATBD/METEOSAT/HEL	Update for MVIRI/SEVIRI Ed. 3
2.1	20/08/2016	SAF/CM/DWD/ATBD/METEOSAT/HEL	Update for DRR 2.8/2.9 and SARAH-2
2.2	29/11/2016	SAF/CM/DWD/ATBD/METEOSAT/HEL	Modifications according DRR2.8/2.9 review comments.
2.3	31/10/2018	SAF/CM/DWD/ATBD/METEOSAT/HEL	Update due to SARAH-2 extension until 2017
3.0	06/05/2020	SAF/CM/DWD/ATBD/SARAH/TCDR	Update for SARAH-3 (MVIRI/SEVIRI ed. 4)
3.1	10/06/2020	SAF/CM/DWD/ATBD/SARAH/TCDR	PCR Review comments included
3.2	15/11/2021	SAF/CM/DWD/ATBD/SARAH/TCDR	Update for SARAH-3 DRR
3.3	28/01/2022	SAF/CM/DWD/ATBD/SARAH/TCDR	DRR Review comments included
3.4	30/01/2023	SAF/CM/DWD/ATBD/SARAH	Including ICDR, in preparation for ORR4.1
3.5	24/02/2023	SAF/CM/DWD/ATBD/SARAH	ORR4.1 Review comments included

	Algorithm Theoretical Basis Document SARAH-3	Doc. No: SAF/CM/DWD/ATBD/SARAH Issue: 3.5 Date: 24.02.2023
---	---	--

Applicable Documents

Reference	Title	Code
AD 1	CM SAF Product Requirements Document	SAF/CM/DWD/PRD/4.1
AD 2	Requirements Review Document	SAF/CM/CDOP3/DWD/RR/38/1 .2


Reference Documents

Reference	Title	Code
RD 1	Algorithm Theoretical Baseline Document, Meteosat (MVIRI) Solar Irradiance and effective Cloud Albedo Climate Data Sets, MVIRI_HEL; The MAGICSOL method	SAF/CM/DWD/ATBD/MVIRI_HEL/1.2
RD 2	Algorithm Theoretical Baseline Document, Spectrally Resolved Solar Surface Irradiance, SRI	SAF/CM/DWD/ATBD/SRI/1.1

Table of Contents

The EUMETSAT SAF on Climate Monitoring (CM SAF).....	9
1 Introduction	11
2 Helsenow	13
2.1 Basic retrieval principle	13
2.2 Cloud movement detection using Optical Flow.....	13
2.3 Retrieving the instantaneous snow mask.....	14
2.4 Retrieving the daily snow mask and its brightness	15
2.5 Correcting for fog-like clouds and false snow detection.....	15
2.6 Special treatment: December 1988.....	16
3 The Heliosat method	17
3.1 The original Heliosat algorithm.....	17
3.2 From Heliosat to MAGIC SOL.....	17
3.3 Self-calibration	17
3.4 Clear sky reflection	18
3.5 Correction for Viewing Geometry	19
3.6 Input data.....	19
3.7 Effective cloud albedo (CAL).....	20
3.7.1 Averaging	21
3.8 Uncertainty of the effective cloud albedo retrieval	21
3.8.1 Sensitivity of the effective cloud albedo on ρ_{\max} and ρ_{sf}	21
3.8.2 Sensitivity of CAL on self-calibration method	22
3.8.3 Sensitivity of CAL on clear sky reflection	22
3.9 Limitations, assumptions and future improvements.....	22
3.10 Relation of the effective cloud albedo to solar irradiance	23
4 The gnu-MAGIC / SPECMAGIC algorithm.....	25
4.1 Solar irradiance: Introduction and Definition.....	25

4.2	Motivation and strategy for solar surface irradiance and direct irradiance	25
4.3	Algorithm Overview.....	26
4.4	Spectral albedo background information	27
4.5	Atmospheric input information.....	27
5	Surface solar radiation parameters.....	29
5.1	Averaging	29
5.2	Sensitivity and dependence on input parameters of SIS / SDI / PAR / DAL	30
5.2.1	Water vapour	30
5.2.2	Ozone.....	30
5.2.3	Aerosols	30
5.2.4	Surface albedo	31
5.2.5	Clear sky index.....	31
5.3	Assumption, limitations and future improvements	32
6	Spectral surface radiation parameters (PAR and DAL).....	33
6.1	Photosynthetic Active Radiation.....	33
6.2	Daylight (DAL)	34
7	Sunshine Duration.....	36
7.1	Weighting of sunny slots	37
7.2	Assumption, limitations and future improvements	38
8	Improvements relative to the released previous versions of the CM SAF Surface Radiation data records.	39
8.1	Improvements compared to the MVIRI Surface Radiation data record.....	39
8.2	Improvements compared to the first version of SARAH data record (MVIRI/SEVIRI Ed.2)	39
8.3	Improvements of SARAH-3 relative to the SARAH-2 data record (MVIRI/SEVIRI Ed.3)	40
9	Adaptions for ICDR generation.....	41
9.1	Algorithmic adaptions.....	41
9.2	Auxiliary data	41

	<p align="center">Algorithm Theoretical Basis Document SARAH-3</p>	<p>Doc. No: SAF/CM/DWD/ATBD/SARAH Issue: 3.5 Date: 24.02.2023</p>
---	---	---

10 References.....42

11 Glossary – List of Acronyms.....46

List of Tables

Table 1-1: Overview of Meteosat based data records discussed in this ATBD. 12

List of Figures

Figure 2-1: Examples of Meteosat visible image (left) and corresponding result of the Farneböck Optical Flow output (right) for the 10th March 2006, 12.30 UTC. Right side: Darker areas mean low mobility (of objects / clouds) between two consecutive images. 14

Figure 2-2: Example of a daily snow mask retrieved by Helsnow for the 10th March 2006. Left: Full Meteosat disk; Right: Focus on Europe. 15

Figure 3-1: Normalized spectral responses for the broadband visible channel of MVIRI and the two visible bands of SEVIRI. Also shown is the normalized solar spectral irradiance (Figure taken from Cros et al., 2006)..... 20

Figure 3-2: The conversion factors, f_{wb} , for the spectral resolved effective cloud albedo as a function of broadband clear sky index, k_b 24

Figure 4-1: The relation of the transmission to a manifold of atmospheric states is pre-calculated with a radiative transfer model (RTM) and saved in a look-up table (LUT). Once, the LUT has been computed the transmittance for a given atmospheric state can be extracted from the LUT for each satellite pixel and time. 26

Figure 5-1: Diagram of the interface of gnu-MAGIC / SPECMAGIC to the atmospheric input and the satellite observations, C_{eff} stands for the dark offset corrected and normalised Counts. 29

Figure 6-1: Spectral weighting of Kato-bands to generate PAR 34

Figure 6-2: Spectral weighting of Kato-bands to generate DAL..... 35

Figure 7-1: Clear sky daylength (h) based on $DNI \geq 120 \text{ W/m}^2$ for 1st of June. 36

Figure 7-2: Demonstration for accounting for surrounding grid points. The target grid point is marked in the centre..... 37

	<p align="center">Algorithm Theoretical Basis Document SARAH-3</p>	<p>Doc. No: SAF/CM/DWD/ATBD/SARAH Issue: 3.5 Date: 24.02.2023</p>
---	---	---

The EUMETSAT SAF on Climate Monitoring (CM SAF)

The importance of satellite-based climate monitoring was recognized in 2000 by EUMETSAT Member States when they amended the EUMETSAT Convention to affirm that the EUMETSAT mandate is also to “contribute to the operational monitoring of the climate and the detection of global climatic changes”. Following this, EUMETSAT established within its Satellite Application Facility (SAF) network a dedicated centre, the SAF on Climate Monitoring (CM SAF, <http://www.cmsaf.eu>).


The consortium of CM SAF currently comprises the Deutscher Wetterdienst (DWD) as host institute, and the partners from the Royal Meteorological Institute of Belgium (RMIB), the Finnish Meteorological Institute (FMI), the Royal Meteorological Institute of the Netherlands (KNMI), the Swedish Meteorological and Hydrological Institute (SMHI), the Meteorological Service of Switzerland (MeteoSwiss), the Meteorological Service of the United Kingdom (UK MetOffice) and the Centre National de la recherche scientifique (CNRS) of France. Since the beginning in 1999, the EUMETSAT Satellite Application Facility on Climate Monitoring (CM SAF) has developed and will continue to develop capabilities for a sustained generation and provision of Climate Data Records (CDR’s) derived from operational meteorological satellites.

In particular, the generation of long-term data records is pursued. The ultimate aim is to make the resulting data records suitable for the analysis of climate variability and potentially the detection of climate trends. CM SAF works in close collaboration with the EUMETSAT Central Facility and liaises with other satellite operators to advance the availability, quality and usability of Fundamental Climate Data Records (FCDRs) as defined by the Global Climate Observing System (GCOS). As a major task, the CM SAF utilizes FCDRs to produce records of Essential Climate Variables (ECVs) as defined by GCOS. Thematically, the focus of CM SAF is on ECVs associated with the global energy and water cycle.

Another essential task of CM SAF is to produce data records that can serve applications related to the new Global Framework of Climate Services initiated by the WMO World Climate Conference-3 in 2009. CM SAF is supporting climate services at national meteorological and hydrological services (NMHSs) with long-term data records but also with data records produced close to real time that can be used to prepare monthly/annual updates of the state of the climate. Both types of products together allow for a consistent description of mean values, anomalies, variability, and potential trends for the selected ECVs. CM SAF ECV data records also serve the improvement of climate models both at global and regional scale.

As an essential partner in the related international frameworks, the CM SAF assumes the role as main implementer of EUMETSAT’s commitments in support to global climate monitoring. This is achieved through:

- Application of highest standards and guidelines as lined out by GCOS for the satellite data processing,
- Processing of satellite data within an international collaboration benefiting from developments at international level and pollinating the partnership with own ideas and standards,

	<p align="center">Algorithm Theoretical Basis Document SARAH-3</p>	<p>Doc. No: SAF/CM/DWD/ATBD/SARAH Issue: 3.5 Date: 24.02.2023</p>
---	---	---

- Intensive validation and improvement of the CM SAF climate data records,
- Taking a major role in data record assessments performed by research organisations such as WCRP (World Climate Research Programme),
- Maintaining and providing an operational and sustained infrastructure that can serve the community within the transition of mature CDR products from the research community into operational environments.

A catalogue of all available CM SAF products is accessible via the CM SAF webpage, www.cmsaf.eu. Here, detailed information about product ordering, add-on tools, sample programs and documentation is provided.

	Algorithm Theoretical Basis Document SARAH-3	Doc. No: SAF/CM/DWD/ATBD/SARAH Issue: 3.5 Date: 24.02.2023
---	---	--

1 Introduction

The generated 38 year long (1983-2020) continuous surface solar radiation climate data records are based on observations from the Meteosat First and Second Generation satellites; it is the third release of the SARAH data record (SARAH-3) and is temporally extended to present with a corresponding Interim Climate Data Record (ICDR) with a timeliness of a few days. The Digital Object Identifier (DOI) of this SARAH-3 data record is 10.5676/EUM_SAF_CM/SARAH/V003.

For climate monitoring and climate analysis time series of climate variables of sufficient length (i.e., spanning multiple decades) are required. To generate such long time series, the satellite information of the first generation of Meteosat satellites (Meteosat-2 to Meteosat-7, covering 1982 to 2005) has to be employed. The MVIRI instrument on-board the Meteosat First Generation satellite is equipped with 3 channels: one broadband channel in the visible spectral range, one channel in the infrared range, and one water vapor channel.

The second generation of Meteosat satellites (Meteosat-8 to (currently) Meteosat-11, covering 2005 to today) is equipped with the Spinning Enhanced Visible and Infrared Imager (SEVIRI) and the Geostationary Earth Radiation Budget (GERB) instrument. The GERB instrument is a visible-infrared radiometer for earth radiation budget studies. It provides accurate measurements of the shortwave (SW) and longwave (LW) components of the radiation at the top of the atmosphere. SEVIRI employs twelve spectral channels, which provide more information of the atmosphere compared to its forerunner. Several retrieval algorithms have been developed to use the additional information gained by the improved spectral information of MSG mainly for nowcasting applications. However, these algorithms cannot be applied to the MVIRI instrument on-board the Meteosat First Generation (MFG) satellites as they use spectral information that is not provided by MFG.

As a consequence, in order to be able to provide a long time series covering more than 20 years, a specific climate algorithm has to be applied to the satellite observations from the First and Second Generation of Meteosat satellites.

The MAGIC SOL method is a combination of the well-established Heliosat method (see Section 2) with the SPECMAGIC clear-sky model, based on the gnu-MAGIC clear sky model. MAGIC SOL does meet the above-mentioned requirements. The method provides the effective cloud albedo and surface irradiance parameters.

The MAGIC SOL method requires as satellite information only the measurements of the broadband visible channel and can therefore be applied across different satellite generations. The application to observations from other geostationary satellites, e.g., GOES and GMS, is also possible. Hence, the MAGIC SOL method has not only the power to provide long time series of ECVs, but also to provide ECVs, which cover the complete geostationary ring.

The basis of the cloud part of the MAGIC SOL method is the Heliosat method, which is well established in the solar energy community. However, modifications of the original Heliosat method were needed to meet the requirements to generate a Climate Data Record. These modifications are discussed in Section 3.3.

Main developments relative to the previously used algorithm (for the generation of SARAH-2) are the following:

To improve the retrieval of the surface solar radiation parameters over snow-covered surfaces, the Heliosat method has been extended by applying an internal snow detection algorithm called Helsnow. To distinguish clouds from snow-covered surfaces, Helsnow is based on the fundamental principle that snow-covered surfaces appear bright, but immobile, while clouds appear bright and mobile. The general issue of misclassifying snow-covered surfaces as clouds caused false detections of clouds in case of snow in SARAH-2, which is reduced with Helsnow used to generate SARAH-3.

There are two new radiation parameters included in SARAH-3: the Photosynthetic Active Radiation (PAR) and Daylight (DAL). Both new parameters are spectral radiation parameters.

New auxiliary data from ERA5 (water vapour, ozone) are used for the processing of SARAH-3 (used to be ERA-Interim in SARAH-2). The data are spatially downscaled (water vapor only) and used in a higher temporal resolution than in the generation of SARAH-2. For the generation of ICDR data, forecast data from the operational ECMWF high-resolution model for water vapour and ozone columns are used. The spectrally-resolved albedo data set is updated and now based on monthly climatological values based on MODIS BRDF parameters.

The main modifications relative to RD 1 and to the first version of the SARAH data record are summarized in Section 6.

The generated long-term continuous surface radiation climate data record is based on observations from the Meteosat First and Second Generation satellites and is called SARAH: Surface Solar Radiation Data record – Heliosat. This document reports the algorithm used to derive the third version of the SARAH data record. An overview of the general retrieval algorithm to generate the SARAH climate data record series is given by Mueller et al., 2015b.

Table 1-1: Overview of Meteosat based data records discussed in this ATBD.

Acronym	Product title	Unit
SIS	Surface Incoming Shortwave Irradiance	W/m ²
CAL	Effective Cloud Albedo	Dimensionless
SDI	Surface Direct Irradiance	W/m ²
SDU	Sunshine Duration	h
PAR	Photosynthetic Active Radiation	μmol m ⁻² s ⁻¹
DAL	Daylight	kLux

	<p align="center">Algorithm Theoretical Basis Document SARAH-3</p>	<p>Doc. No: SAF/CM/DWD/ATBD/SARAH Issue: 3.5 Date: 24.02.2023</p>
---	---	---

2 Helsnow

The so-called Helsnow algorithm is a method developed to detect snow-covered pixels in the Meteosat field of view, with the goal of an improved retrieval of surface radiation parameters.

The main output of Helsnow is a daily snowmask with surface reflectivity values attached to each pixel classified as snow-covered. In the case of snow, the actual surface reflectivity is used in the Heliosat method to better account for snow in the retrieval of the surface incoming radiation parameters. Helsnow has been developed in a cooperation between the CM SAF, University of Mainz and the rmags GmbH.

2.1 Basic retrieval principle

The idea behind Helsnow is simple: Comparably bright pixels represent either cloudy pixels or (clear sky) pixels with snow-covered surfaces. However, as clouds are typically changing / moving in time, bright immobile pixels are likely to be snow-covered and not cloudy. An exception is fog - bright and quite immobile – which receives an extra treatment in Helsnow. Helsnow is running month by month, throughout the year. As a result a daily snow mask is generated together with information on the snow brightness / reflectance. Both information is then used in the Heliosat algorithm as the surface reflectance to better account for snow-covered surfaces in the satellite retrieval.

2.2 Cloud movement detection using Optical Flow

As a first step in Helsnow, the movements of clouds (and basically of all objects) is determined by using the Farneback Optical Flow method (Farneback, 2003) with its part of the OpenCV Software package (openCV.org). Thereby the movement of objects is calculated from one Meteosat satellite image to another using the Meteosat visible channels. Moving objects (pixels) are detected and excluded from the further snow detection processing steps, and later processed like in the classical Heliosat approach. Very slow moving objects are further analyzed in the next steps. The threshold to distinguish between immobile and mobile objects has been determined by sensitivity studies. This threshold speed is different for the MVIRI and SEVIRI instruments, as their native spatial resolutions are different.

Objects and pixels classified as immobile represent clear-sky conditions, hence the view on the Earth's surface is potentially possible. Figure 2-1 shows as an example the result of the Optical Flow calculation using the Farneback algorithm. In general cloud-free areas (left part of Figure 2-1) have correctly been identified and appear dark (low mobility / cloud movement). It can also be seen that the algorithm is quite sensitive also for thin clouds, which is intended to avoid cloud contaminations in the cloud-free pixels.

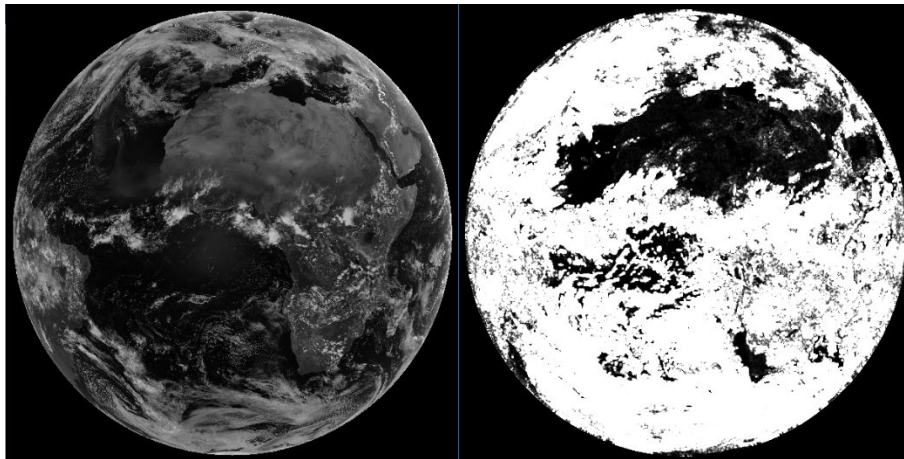


Figure 2-1: Examples of Meteosat visible image (left) and corresponding result of the Farneback Optical Flow output (right) for the 10th March 2006, 12.30 UTC. Right side: Darker areas mean low mobility (of objects / clouds) between two consecutive images.


2.3 Retrieving the instantaneous snow mask

As an initial step to detect snow, the determination of annual clear-sky snow-free background fields (YCS fields) is required. These data are used to determine whether a certain pixel can be considered as ‘bright’ in the Helsnow processing. The YCS fields are derived by calculating a robust minimum brightness for each pixel using data for the months of June, July and August for each year. For the YCS field generation it is important to exclude snow. As snow plays a minor role in the Southern Hemisphere of the METEOSAT field of view, the Northern Hemisphere’s summer based YCS fields are applied for the full disk.

Those YSC fields are then used to derive the instantaneous snow masks by comparing the current brightness of immobile pixels to the YCS fields. As initial value for the snowmask of the first day of a month, the snowmask from a backward propagating loop of that month is used. To avoid inconsistencies in the snowmask at the change from month-to-month, the “monthly” snowmask processing loops +/-5 days beyond the respective month. If the current pixel brightness is greater (by at least 50%) than the YCS brightness of that pixel, the pixel is classified as potentially snow-covered at that point in time. For latitudes lower -50°N and higher +50°N the 50%-threshold is continuously increased to account for the slant viewing geometry. For cloudy pixels, the instantaneous snow mask is not modified and kept constant.

The detection loop over satellite images is done forward and backward in time in order to avoid problems (like missing data) at the beginning and end of a (monthly) loop. As additional information, a land-sea mask is used to mask out snow over oceans.

The snow cover and brightness information derived from Helsnow is only used for the retrieval of the surface radiation for days with a successful detection of snow cover at that day and that pixel. This in turn means, that the snow cover information is only used in case of mainly sunny days when the effect of snow is most relevant.

	<p align="center">Algorithm Theoretical Basis Document SARAH-3</p>	<p>Doc. No: SAF/CM/DWD/ATBD/SARAH Issue: 3.5 Date: 24.02.2023</p>
---	---	---

2.4 Retrieving the daily snow mask and its brightness

Based on the instantaneous snow mask, the daily snow mask is calculated. To do so, the number of instantaneous snow detections during a day are counted. Pixels that have been classified as being snow-covered for more than two thirds of the day (between 9 and 15.30 UTC) are classified as being snow-covered for that day. The brightness of the snow / the surface is determined as the average brightness of the snow-covered pixels at that day, and later also used as important information in the Heliosat method (see Section 3). If an update of the daily snow mask is not possible for a certain pixel (e.g., due to cloud coverage), no snow cover information is used in the radiation retrieval and the pixel is treated as 'non snow covered'. Figure 2-2 shows an example daily snowmask for the 10th March 2006, which includes not only information on snow (yes/no), but also information on the snow brightness, which is required for the estimation of CAL, and, consequently, for the surface radiation parameters.

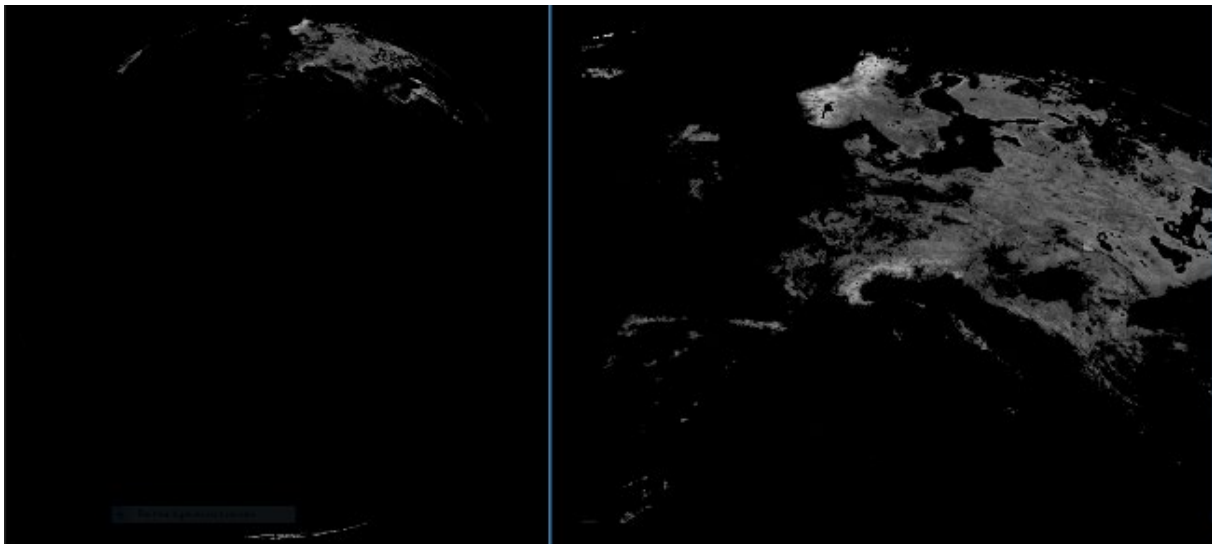


Figure 2-2: Example of a daily snow mask retrieved by Helsnow for the 10th March 2006. Left: Full Meteosat disk; Right: Focus on Europe.

2.5 Correcting for fog-like clouds and false snow detection

Bright and comparable immobile clouds (e.g., fog) are difficult to detect by the Helsnow algorithm and to separate from snow-covered surfaces. To reduce the misclassification of fog as snow, a check and correction for fog is done based on the instantaneous and the daily snow mask.

Compared to snow-covered surfaces, fog often appears brighter and spatially more homogeneous. We use these two characteristics to apply a fog filtering to the daily snow masks. This correction filters out erroneous snow detection in case of very bright and spatially homogeneous areas, which likely are foggy areas. This is done by a two-step approach by applying different thresholds of the mean brightness in a certain area and its variance. For

	<p align="center">Algorithm Theoretical Basis Document SARAH-3</p>	<p>Doc. No: SAF/CM/DWD/ATBD/SARAH Issue: 3.5 Date: 24.02.2023</p>
---	---	---

relatively dark pixels (still only pixels that have been detected as potentially snow-covered are considered) the filter is more strict and only filters very homogeneous areas. In a second step, brighter pixels are filtered out by using a less strict homogeneity threshold. This second step is set up in order to keep bright snow in mountainous regions (that is mostly quite bright and heterogeneous) but shall remove bright foggy areas.

To further correct for wrongly detected snow cover, e.g. due to misclassification of fog as snow coverage, a snow mask is generated based on data from the ECMWF reanalysis system. Spatially high resolution daily (12 UTC) snow cover data is used from the ERA5-Land data record ('snowc') (Muñoz-Sabater et al., 2021) to identify possible snow-covered grid pixels over land, daily information on the sea ice fraction is used from the ERA5 data record ('siconc'). Both data records are combined and remapped to the SARAH-3 grid; these data are used as an additional mask to ensure that only those grid points are treated as snow-covered in the SARAH-3 retrieval, which are covered with snow / sea ice also in the ECMWF ERA reanalysis system. This additional masking substantially reduces the false snow detections without removing correctly identified snow cover.

2.6 Special treatment: December 1988

Only very limited visible channel MVIRI data from December 1988 are available in the archive for the processing of the SARAH climate data record. In particular, for many days less than 50% of the daytime slots are available throughout this month; as a consequence, the HELSNOW algorithm cannot be applied for December 1988. To avoid misclassification of snow-covered pixels with cloudy pixels ERA5 data were used to identify those grid points with daily low cloud coverage and snow coverage. These grid points were set to missing value in the SARAH-3 data record.

	<p align="center">Algorithm Theoretical Basis Document SARAH-3</p>	<p>Doc. No: SAF/CM/DWD/ATBD/SARAH Issue: 3.5 Date: 24.02.2023</p>
---	---	---

3 The Heliosat method

3.1 The original Heliosat algorithm

The Heliosat algorithm uses reflection measurements given as normalized digital counts to determine the effective cloud albedo, also called cloud index (Beyer et al. 1996; Cano et al. 1986; Hammer et al. 2003). A clear sky model is used afterwards to calculate the solar surface irradiance based on the retrieved effective cloud albedo. Basis of the Heliosat method are the digital counts of the visible Meteosat channel. No information from NIR or IR channels is required.

The first step in the Heliosat method is the retrieval of the effective cloud albedo (cloud index), n , i.e. the normalised relation between the all sky and the clear sky reflection in the visible channel observed by the satellite:

Equation 3-1
$$n = \frac{\rho - \rho_{sfc}}{\rho_{max} - \rho_{sfc}}$$

Here, ρ is the observed reflection for each pixel and time in counts. ρ_{sfc} is the clear sky reflection, and ρ_{max} is an estimate for the maximum reflectivity observed by the satellite.


3.2 From Heliosat to MAGIC SOL

To meet the requirements of a CDR some modifications of the original Heliosat algorithm have been performed, resulting in a version of the Heliosat algorithm for the generation of climate data records. In particular a self-calibration algorithm (see Section 3.3), which dynamically accounts for changes in sensor sensitivity, has been developed. The modified version of the Heliosat algorithm in combination with the gnu-MAGIC / SPECMAGIC approach (see Section 4) is called MAGIC SOL.

The MAGIC SOL approach has been used in the processing of the CM SAF Surface Radiation data record based on the MVIRI instruments on-board the first generation of Meteosat satellites (Posselt et al., 2012). Full details of the algorithm are presented in RD 1, Posselt et al. (2012) and Müller et al. (2015). Here an overview of the method is provided.

3.3 Self-calibration

The self-calibration algorithm is based on Rigollier et al., (2002) an operational and automatic determination of the maximum reflectivity ρ_{max} . A histogram of all available counts is generated and the 95th-percentile is used as self-calibration parameter and set to ρ_{max} (Hammer et al., 2003 and references therein). Only satellite pixels located in the southern Atlantic between 15° W and 0° W and 58° S and 48° S are considered. This region features a high abundance of frontal systems with large cloud amounts most of the time, but hardly any convection. The statistical analysis is based on one month of satellite data at 13 UTC. The resulting estimate for ρ_{max} is then applied to all slots within that month.

	Algorithm Theoretical Basis Document SARAH-3	Doc. No: SAF/CM/DWD/ATBD/SARAH Issue: 3.5 Date: 24.02.2023
---	---	--

Further details and a validation of the self calibration method can be found in Posselt et al. (2012) and RD 1.

3.4 Clear sky reflection

The processing of the long time series of surface solar radiation from the geostationary Meteosat satellites employs a robust clear sky or background reflection method based on Hammer (2000). This method replaces the method of (Dürr and Zelenka 2009), which was used in the processing of the CM SAF MVIRI-based surface radiation data record (Posselt et al., 2012). While the previously used method works well over snow covered regions, it has some weakness over desert regions. In SARAH-3, the combination of the classical Hammer (2000) Heliosat method together with Helsnow is used.

The clear sky reflection is derived from the frequency distribution of the observed reflections during an appropriate time period. This frequency distribution exhibits one peak for cloudy and a separate peak for clear sky reflection. The peak for clear sky reflection is usually significantly lower and at the lower end of the overall frequency distribution, the dark counts. Hence, the clear sky reflection can be estimated by a minima approach. Using the lowest value of the reflection within a certain time period might be an option. However, the lowest values are often a result of cloud shadows and therefore do not represent the clear sky reflection. Hence, the clear sky reflection can be interpreted as a stationary variate with a mean value ρ_{sfc} and a variance ε . All values above a starting value ρ_{sfc} plus the ε are iteratively sorted out. After each iteration step a new mean is derived, hence a new limit for the sorting applies.

The iteration process is given in Equation 3-2, the calculated mean iterates to the clear sky reflection ρ_{sfc} if Equation 3-3 is fulfilled. Here ρ_{cld} and ε_{cld} are the respective values for clouds:

$$\begin{aligned}
&\text{starting value : } \rho_{srf} = \max(\text{datarange}) \\
&\text{iteration : if } (\rho < \rho_{srf} + \varepsilon) \rightarrow \rho_{srf} = \rho \\
&\hspace{10em} (\text{change}) \\
&\text{else : } \rightarrow \rho_{srf} = \rho_{srf} \\
&\hspace{10em} (\text{no change})
\end{aligned}$$

Equation 3-2

$$\rho_{cld} - \rho_{srf} > \max(\varepsilon, \varepsilon_{cld})$$

Equation 3-3

The clear sky reflection is derived for every snow free pixel and every slot. The time series has to be long enough to contain cloudless conditions for every pixel. However, the time series should be also short enough to consider seasonal changes in the surface albedo. Hence, a time span of about 1 month is assumed to be appropriate and widely used. The surface albedo exhibits a strong dependency on the solar zenith angle. The surface albedo in turn is the driving factor for the clear sky reflection. Hence, the method is applied for every slot, in order to resolve the solar zenith angle dependency. As the mean of the dark counts is used, values of CAL smaller than 0 might occur.

In case snow has been detected by HELSNOW, the daily mean snow brightness for a given day and pixel is used as ρ_{srf} . This accounts for the existence of snow in the derivation of CAL.

	Algorithm Theoretical Basis Document SARAH-3	Doc. No: SAF/CM/DWD/ATBD/SARAH Issue: 3.5 Date: 24.02.2023
---	---	--

3.5 Correction for Viewing Geometry

Due to the longer atmospheric path to the satellite sensor, the detection of clouds is artificially enhanced at larger satellite zenith angles resulting in an underestimation of surface solar radiation in the outer regions of the Meteosat disc. This effect is empirically parameterized as a function of the satellite zenith angle, Θ_{sat} :

Equation 3-4 $Corr = 0.1 * \left(\cos\left(\frac{\Theta_{sat}}{1.13}\right)^{1.3} \right)^{-0.9} - 1$

To apply the correction factor only under moderate CAL conditions, the correction is applied for $CAL > 0.04$ and $CAL * \Theta_{sat} / 1.3 < 0.55$:

Equation 3-5 $n = n * (1 - Corr)$

3.6 Input data

From the MVIRI instruments on-board the first generation of Meteosat satellites the rectified digital pixel counts of the broadband visible MVIRI channel are used. The respective data are called “Rectified Image Data” and provided by EUMETSAT (EUM TD 06) in openMTP format. However, other formats and satellite images can be treated as well. Rectified images containing counts are used.

The SEVIRI instruments on-board the Second Generation of Meteosat Satellites do not continue to provide the same spectral broadband information as the MVIRI instruments. For a consistent prolongation of the time series from the MVIRI instruments to the SEVIRI instruments a broadband conversion has to be used for SEVIRI (Posselt et al., 2011). A linear combination of the MSG/SEVIRI visible narrowband channels (VIS006 and VIS008) will be used (Cros et al., 2006, see Figure 3-1). This approach has been proven to enable a homogeneous retrieval of surface solar radiation between MFG and MSG (Posselt et al., 2013).

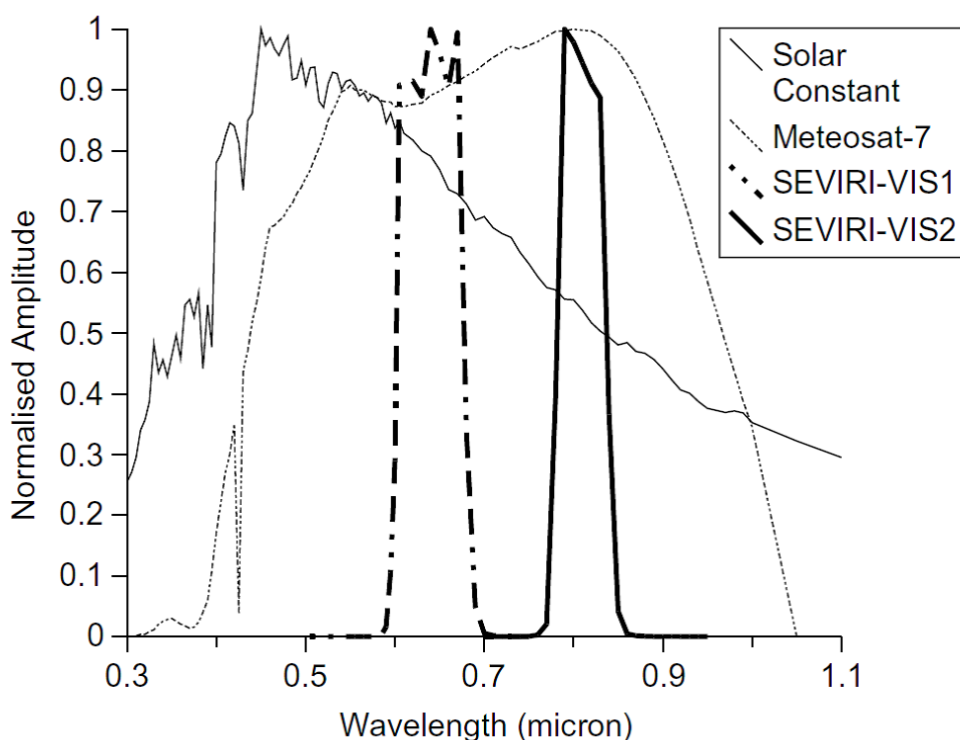


Figure 3-1: Normalized spectral responses for the broadband visible channel of MVIRI and the two visible bands of SEVIRI. Also shown is the normalized solar spectral irradiance (Figure taken from Cros et al., 2006).

The first MVIRI climate data record of CM SAF shows stripe artefacts in the radiation products, due to similar features in the MVIRI raw images. Starting with SARAH-1, all MVIRI raw images covering the time period 1983-1994 have been visually inspected. For SARAH the missing scan lines have been filled by spatial-temporal interpolation in order to have sufficient images for the processing and to gain the optimal information content out of the images. Images with unfixable bugs have been identified and have been not used for the processing.

The ECMWF Reanalysis Version 5 (ERA5) is the latest global reanalysis by ECMWF. Over land areas, the ERA5-Land reanalysis is available as well, having a higher spatial resolution than ERA5. Within HELSNOW, the combination of the daily datasets of ERA5-Land snow cover and ERA5 sea ice are fraction are used. The data is re-gridded onto the native MVIRI/SEVIRI grid and used to mask out false detections of snow by HELSNOW.

3.7 Effective cloud albedo (CAL)

The effective cloud albedo is derived with the MAGIC SOL method described in the previous sections. Clouds have a net cooling effect, which is several magnitudes higher than the forcing caused by the increase of greenhouse gases. Every trend and anomalies in the effective cloud albedo would significantly affect the climate system on a global and/or regional scale. However, despite its relevance for the climate system, it has not yet been classified as an essential climate variable by GCOS. As clouds can be assumed as Lambertian surfaces, the derived quantity can be considered the effective cloud albedo.

	Algorithm Theoretical Basis Document SARAH-3	Doc. No: SAF/CM/DWD/ATBD/SARAH Issue: 3.5 Date: 24.02.2023
---	---	--

It is important to note that the effective cloud albedo does depend on the cloud reflectivity and the surface albedo. The same cloud has a larger effective cloud albedo over a dark surface (e.g., ocean) than over a bright surface (e.g., desert). For the assessment of the radiative impact of clouds on the reflected solar radiation the effective cloud albedo is the relevant cloud radiative property.

3.7.1 Averaging

Monthly and daily means of the effective cloud albedo are calculated by arithmetic averaging, using Equation 3-6:

Equation 3-6

$$CAL_{mean} = \frac{\sum_{i=1}^n CAL_i}{n}$$

Here n corresponds to the number of available instantaneous cloud albedo data per day for the calculation of the daily mean or to the number of available daily means for the calculation of the monthly means. A minimum value of 25% instantaneous cloud albedo data sets per day available is required to derive the daily mean for this specific pixel. The required minimum number of CAL measurements for the calculation of the daily means is a compromise between accuracy requirements and resulting data availability. The monthly average is calculated from the daily means for each pixel as the arithmetic mean following the WMO criteria to calculate monthly means, i.e., the monthly average is not calculated if more than ten daily values or five or more consecutive daily values are missing (WMO, 2018).

The conversion from the irregular satellite projection to the regular 0.05 x 0.05 degree regular lon-lat-grid is conducted with the gnuMAGIC gridding tool based on a nearest-neighbour method.

3.8 Uncertainty of the effective cloud albedo retrieval

The uncertainty associated with the retrieval of the effective cloud albedo can be estimated based on the sensitivity of CAL on the parameters used in the retrieval of CAL. Here the main results of the sensitivity assessment are summarized; details are found in RD 1.

3.8.1 Sensitivity of the effective cloud albedo on ρ_{max} and ρ_{srf}

The effective cloud albedo is defined as a relative quantity of observed satellite counts. Hence, any noise or uncertainty in the absolute calibration of the satellite observations cancels out. The uncertainty in the effective cloud albedo is therefore pre-dominantly determined by uncertainties in the determination of the clear sky reflection and the self-calibration method.

	Algorithm Theoretical Basis Document SARAH-3	Doc. No: SAF/CM/DWD/ATBD/SARAH Issue: 3.5 Date: 24.02.2023
---	---	--

3.8.2 Sensitivity of CAL on self-calibration method

The uncertainty or fuzziness in ρ_{\max} defined by the month to month variations of ρ_{\max} is in the order of 3%. However, it is likely that part of this uncertainty is due to the variability in the satellite counts, which will cancel out in the calculation of the effective cloud albedo (Equation 3-1), and, hence, do not affect the accuracy of CAL. Under the worst case assumption of an uncertainty of ρ_{\max} of 3% the uncertainty of CAL is in the order of 5 % over bright surfaces. However, such high uncertainties occur only for high CAL values, hence the effect on solar irradiance is rather low. Further information can be found in RD 1.

3.8.3 Sensitivity of CAL on clear sky reflection

The impact of the uncertainty in the determination of the clear sky reflection on the effective cloud albedo is low because of the occurrence of ρ_{srf} in the dominator and nominator of the effective cloud albedo formula.

However, the clear sky reflection can introduce significant uncertainty in the effective cloud albedo retrieval for the case of cloud contamination. This happens if not enough clear sky cases occur. Hence, for regions with long-lasting cloud cover in combination with slant geometry the ρ_{srf} retrieval fails to see the clear sky situations, hence ρ_{srf} is contaminated by clouds and not fully representative for clear sky conditions. This effect occurs pre-dominantly at the border of the Meteosat disk, above 60 degrees viewing angle. As it occurs only for regions with long-lasting cloud coverage (hence large values of the effective cloud albedo) the effect on the solar irradiance is much lower as implied by the uncertainty in the effective cloud albedo. Further information and graphical illustrations of these effects can be found in RD 1.

3.9 Limitations, assumptions and future improvements

Below is a list of some known deficiencies and limitations of the algorithm to derive CAL:

- The clear sky reflection, ρ_{sfc} , can accurately be retrieved if a certain number of clear sky cases are available within a month. This is not always the case.
- Snow-covered surfaces might still be interpreted as clouds by the algorithms, resulting in an overestimation of the effective cloud albedo under these situations. The severity of this issue has been reduced by introducing HELSNOW in SARAH-3.
- Neglecting the anisotropic reflection of clouds introduces some uncertainty to the derived effective cloud albedo. While this assumption is thought to be a good approximation for low level water clouds, the scattering function of high level ice clouds might not follow this assumption.

3.10 Relation of the effective cloud albedo to solar irradiance

The ratio of the all-sky surface solar radiation and the clear-sky surface solar radiation is the clear sky index:

Equation 3-7 $k = SIS / SIS_{CLS}$

Hence, the all-sky surface solar radiation can be derived as the product of the clear-sky index and the clear-sky surface solar radiation:

Equation 3-8 $SIS = k \cdot SIS_{CLS}$

Here SIS_{CLS} is the solar irradiance for cloud free skies. For most conditions, the effective cloud albedo, CAL, can be related to the clear sky index by:

Equation 3-9 $k = 1 - CAL$

This relation is defined by the law of energy conservation (Dagestad, 2004). For CAL values below -0.2 and above 0.8 empirical corrections are required:

Equation 3-10

$CAL < -0.2:$		$k=1.2$
$-0.2 < CAL < 0.8$		$k = 1 - CAL$
$0.8 < CAL < 1$	$k = 2.0667 - 3.6667 \cdot CAL + 1.6667 \cdot CAL^2$	
$CAL > 1.1$		$k = 0.05$

Based on the diffuse model of Skartveit et al. (1998) the direct solar radiation, SID, is derived from the clear-sky index using the following formula

Equation 3-11 $SID = SID_{CLS}(k - 0.38 \cdot (1 - k))^{2.5}$

For values of the cloud albedo larger than 0.6 the direct irradiance is zero, which is in line with observations (Skartveit et al., 1998). The direct normalized irradiance, DNI, is derived from SID by normalisation with the cosine of the solar zenith angle (SZA):

Equation 3-12 $DNI = SID / \cos(SZA)$

To account for the spectral dependency of the cloud effect described by the clear-sky index, the broadband spectral index, k, is adjusted to result in a spectral dependent clear sky index k^{wb} , for each of the considered 32 wavelength bands. These conversion factors, f^{wb} , have been determined for different values of the cloud albedo using radiative transfer calculations with the RTM libradtran and are shown in Figure 2-1. The spectrally resolved clear sky index, k^{wb} , can then be derived from the broadband clear sky index:

Equation 3-13 $k^{wb} = f^{wb} \cdot k$

The spectrally resolved irradiance is finally derived by application of Equation 3-14

Equation 3-14 $SIS^{wb} = k^{wb} \cdot SIS_{cls}^{wb}$

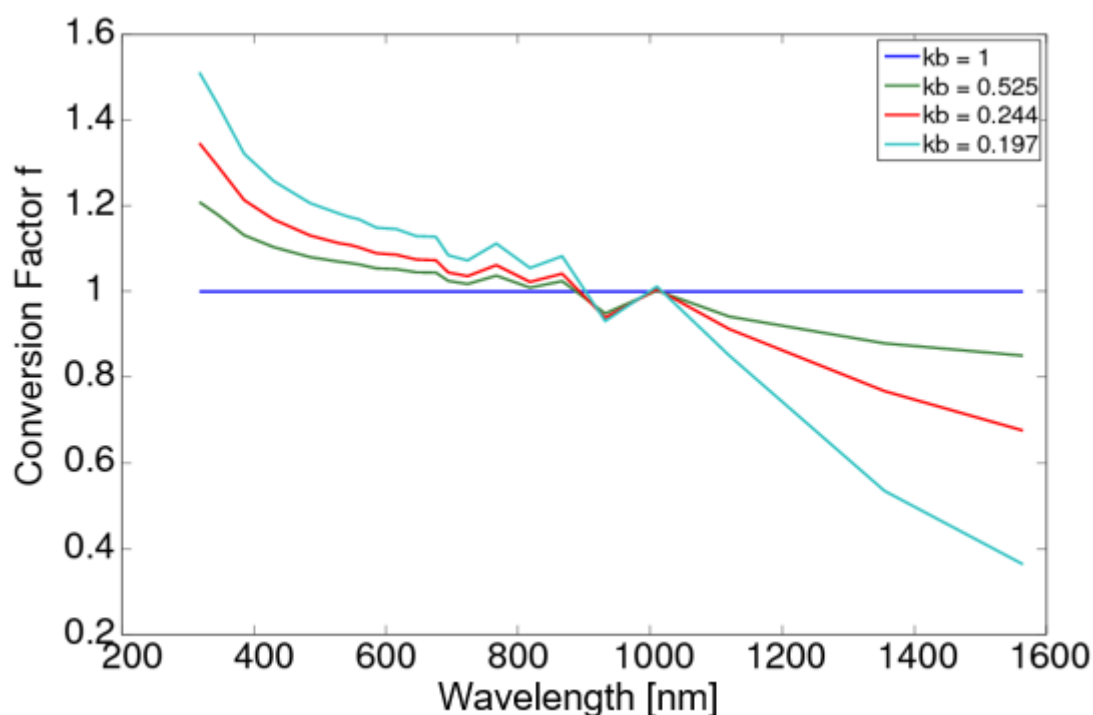


Figure 3-2: The conversion factors, f_{wb} , for the spectral resolved effective cloud albedo as a function of broadband clear sky index, k_b .

More details on the calculation of the spectrally-dependent clear sky index can be found in RD 2 and Mueller et al. (2012).

With the knowledge of the wavelength-dependent clear sky index and the clear sky surface radiation components (global and direct), the all sky surface solar radiation can be derived using the equations given above. The clear sky solar irradiance is calculated using an eigenvector look-up table method (see Mueller et al. 2012; Mueller et al. 2009). It is based on radiative transfer modelling and enables the use of extended information about the atmospheric state. Further details of the clear sky atmospheric radiative transfer model are presented in Section 4.

	Algorithm Theoretical Basis Document SARAH-3	Doc. No: SAF/CM/DWD/ATBD/SARAH Issue: 3.5 Date: 24.02.2023
---	---	--

4 The gnu-MAGIC / SPECMAGIC algorithm

The clear sky solar irradiance is calculated using an eigenvector look-up table method (see Mueller et al. 2012; Mueller et al. 2009). It is based on radiative transfer modelling and enables the use of extended information about the atmospheric state. Accurate analysis of the interaction between the atmosphere, clear sky reflection, transmission and the top of atmosphere albedo has been the basis for this method, characterized by a combination of parameterizations and “eigenvector” look-up tables. A detailed description of the gnu-MAGIC algorithms can be found in RD 1 and Mueller et al. (2009); the extension of gnu-MAGIC, SPECMAGIC, to consider the spectral information and to derive the spectral resolved surface irradiance is described in RD 2 and Mueller et al. (2012).

4.1 Solar irradiance: Introduction and Definition

The solar surface irradiance consists of a diffuse fraction and a direct fraction. The diffuse fraction of the surface irradiance is defined as the solar radiation that has undergone scattering in the atmosphere. The direct irradiance is the flux reaching a horizontal unit of the earth’s surface in the 0.2 - 4 μm wavelength band from the direction of the sun without being scattered. Both quantities are expressed in W/m^2 .

4.2 Motivation and strategy for solar surface irradiance and direct irradiance

Accurate information on the direct and total solar irradiance is important for

- the monitoring, the analysis and the understanding of the climate system,
- the prediction of energy yield, the planning, monitoring and system design of photovoltaic systems and solar-thermal power plants
- agrometeorological applications.

Only a very limited number of well-maintained ground measurements of irradiance (in particular of direct irradiance) exist in Europe, while in Africa and over the ocean almost no information on surface radiation is available from surface observations. Geostationary satellites enable the retrieval of area-wide total and direct irradiance in high spatial and temporal resolution with good accuracy ($<15 \text{ W}/\text{m}^2$).

In the previous years, CM SAF has already successfully extended and applied well-established methods used within the Solar Energy community (e.g., Skartveit et al., 1998) to generate surface solar radiation data records from satellite observations. One important extension of the clear sky surface radiation algorithm (gnu-MAGIC) is the use of detailed aerosol information instead of turbidity maps. The clear sky irradiance is completely based on Radiative Transfer Modelling. Finally, the possibility to use an improved cloud mask is expected to improve the accuracy. The physical basis of the algorithm is described in Mueller et al. (2009) and Müller et al. (2003).

4.3 Algorithm Overview

In the following the gnu-MAGIC / SPECMAGIC algorithm to derive the direct and the spectrally-resolved total surface radiation under clear sky conditions is briefly presented. A full description can be found in RD 1, RD 2, Mueller et al. (2009), and Mueller et al. (2012).

The calculation of the surface clear sky direct irradiance and the surface clear sky solar surface irradiance is realised using an eigenvector look-up table (LUT) approach. The LUTs for the surface direct and total solar radiation have been generated by conducting radiative transfer model (RTM) simulations using libRadtran (Mayer and Kylling, 2005) (Figure 4-1). A LUT is a data structure used to replace the time-consuming RTM computation with a simpler and faster interpolation operation within discrete pre-computed RTM results.

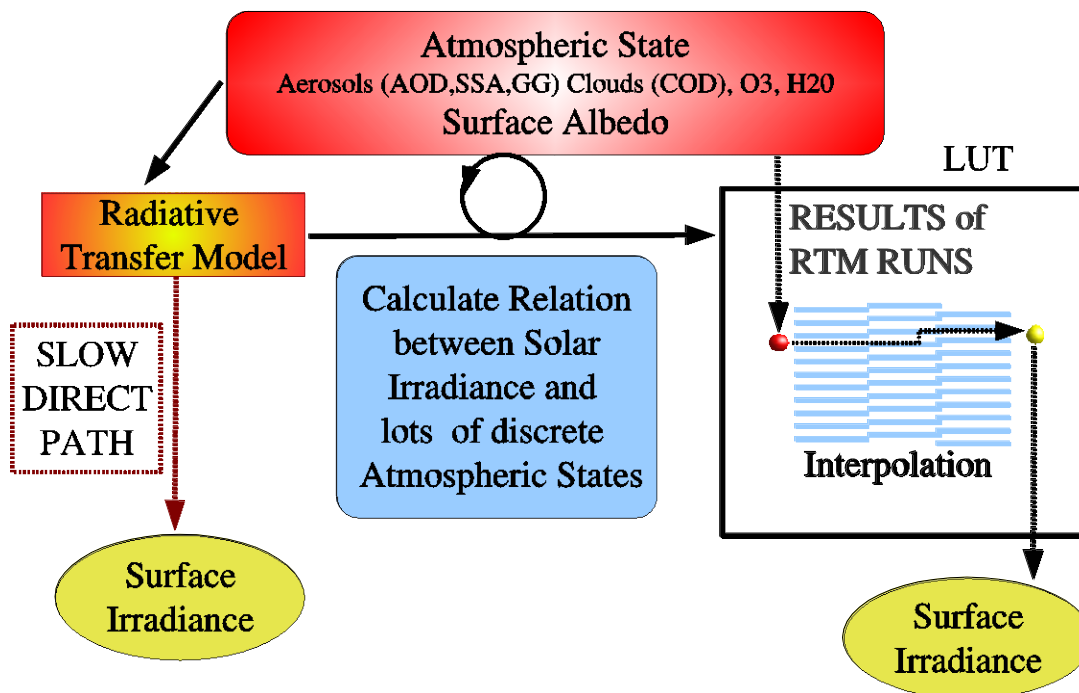


Figure 4-1: The relation of the transmission to a manifold of atmospheric states is pre-calculated with a radiative transfer model (RTM) and saved in a look-up table (LUT). Once, the LUT has been computed the transmittance for a given atmospheric state can be extracted from the LUT for each satellite pixel and time.

The clear sky LUTs consists of radiative transfer model results for aerosols with different aerosol optical thickness, single scattering albedo, and asymmetry parameter. Fixed values for water vapour, ozone and surface albedo have been used for the calculation of the basis LUT. The effect of the solar zenith angle on the transmission, hence the surface solar irradiance, is considered by the use of the Modified Lambert Beer (MLB) function (Mueller et al., 2004). The effects of water vapour and surface albedo on the surface radiation are considered using correction formulas and parameterizations. Therefore the MAGIC code is fast, robust and suitable for operational application.

	<p align="center">Algorithm Theoretical Basis Document SARAH-3</p>	<p>Doc. No: SAF/CM/DWD/ATBD/SARAH Issue: 3.5 Date: 24.02.2023</p>
---	---	---

The input parameters of the gnu-MAGIC / SPECMAGIC code are date, time, solar zenith angle, latitude, longitude, effective cloud albedo (cloud index), water vapour column density, surface albedo, aerosol optical thickness and single scatter albedo for aerosols. The output of the gnu-MAGIC / SPECMAGIC code is the spectrally-resolved (32 kato bands, see also Kato et al., 1999), the total and the direct clear sky surface solar irradiance in the 0.2-4.0 μm wavelength region. The extra-terrestrial total solar irradiance is set to 1361 W/m^2 and adjusted according to the earth-sun distance. More details on the gnu-MAGIC / SPECMAGIC algorithm are described by Mueller et al. (2004, 2009, 2012).

4.4 Spectral albedo background information

Monthly climatological surface albedo information is used with SPECMAGIC based on the data provided by Blanc et al., 2018. These data are based on retrievals of the Bi-directional reflectance distribution function (BRDF) estimated from the MODIS instruments. The surface reflectance is provided at a spatial resolution of 0.05° for 5 spectral bands. The information from the 5 spectral bands has been transferred to match the Kato-bands in the SPECMAGIC clear sky RTM. It is worth noting that surface albedo data with a substantially coarser spatial resolution was used in the generation of previous version of the SARAH data records.


4.5 Atmospheric input information

Here the atmospheric input information used to retrieve the clear sky surface solar irradiance is described. A main change from SARAH-2 to SARAH-3 is the update of atmospheric input data, i.e. the update from ERA-Interim (Dee et al., 2011) to the ERA5 (Hersbach et al., 2020) reanalysis. Thereby also the temporal resolution of atmospheric input has been increased from monthly to daily data for water vapour and ozone.

Aerosol:

Aerosol particles have a significant effect on the surface solar irradiance, because they scatter and absorb solar radiation. To describe the effect of scattering and absorption, information about the aerosol type and aerosol optical depth is needed. The aerosol type determines the relation between scattering and absorption, which is expressed by the single scattering albedo. The asymmetry parameter depends also on the aerosol type (size and composition) and determines the relation between forward- and backward-scattering. For the calculation of direct irradiance only the aerosol optical depth is relevant, as the AOD is defined as the attenuation of direct irradiance. The single scattering albedo and the asymmetry factor (both are determined by the aerosol type) are of relevance for the total solar irradiance (diffuse + direct irradiance).

Monthly mean aerosol information is taken from an aerosol climatology by the European Centre for Medium Range Weather Forecast – MACC (Monitoring Atmospheric Composition and Climate). The MACC data results from a data assimilation system for global reactive gases, aerosols and greenhouse gases. It consists of a forward model for aerosol composition and dynamics (Morcrette et al., 2009) and the data assimilation procedure described in detail in (Benedetti et al., 2009). It has been used for the estimation of aerosol radiative forcing

	Algorithm Theoretical Basis Document SARAH-3	Doc. No: SAF/CM/DWD/ATBD/SARAH Issue: 3.5 Date: 24.02.2023
---	---	--

(Bellouin et al., 2013). The MACC reanalysis data is generated on a Gaussian T159 grid which corresponds to ~120 km resolution. For the use within CM SAF it has been regridded to a 0.5x0.5 degree regular latitude-longitude grid.

The MACC aerosol information has been evaluated to perform better than the Kinne et al. and GADS/OPAC climatology (Hess et al., 1998, Köpke et al. 1997), see Mueller and Träger-Chatterjee (2014) for further details. The original MACC climatology has been adjusted to account for the detection of high aerosol loadings in the cloud index retrieval based on the study of Mueller et al. (2015).

Water vapour:

Water vapour is an important atmospheric absorber in the solar spectral range. Daily values of the vertically-integrated water vapour in a spatial resolution of 0.25° lat/lon are taken from the ERA5 global reanalysis data record of ECMWF/Copernicus (C3S, 2017). A topographic correction is applied when regridding the integrated water vapour from ERA5 to 0.05° lat/lon assuming a scale height of 1600 m based on Bento (2016).

Ozone:

Ozone is a strong absorber in the UV spectral range, but the absorption is quite weak within the broadband spectrum, which is relevant for the estimation of the direct irradiance. Here daily mean values of the total integrated ozone column from ERA5 (C3S, 2017) are used in a spatial resolution of 0.25° lat/lon.

All these external input parameters to the clear sky surface radiation algorithms are spatially interpolated to the satellite observations and used in the gnu-MAGIC / SPECMAGIC algorithm to derive the clear sky direct and the clear sky total surface radiation for every satellite measurement and each satellite pixel. The same holds for the spectral products.

5 Surface solar radiation parameters

To derive the surface solar radiation under all-sky conditions, the clear sky information as derived from the SPECMAGIC algorithm (see Section 4) is combined with the information from the effective cloud albedo (see Section 3) using the formulas presented in Section 3.10. Figure 5-1 presents a schematic overview of the retrieval concept and the algorithm.

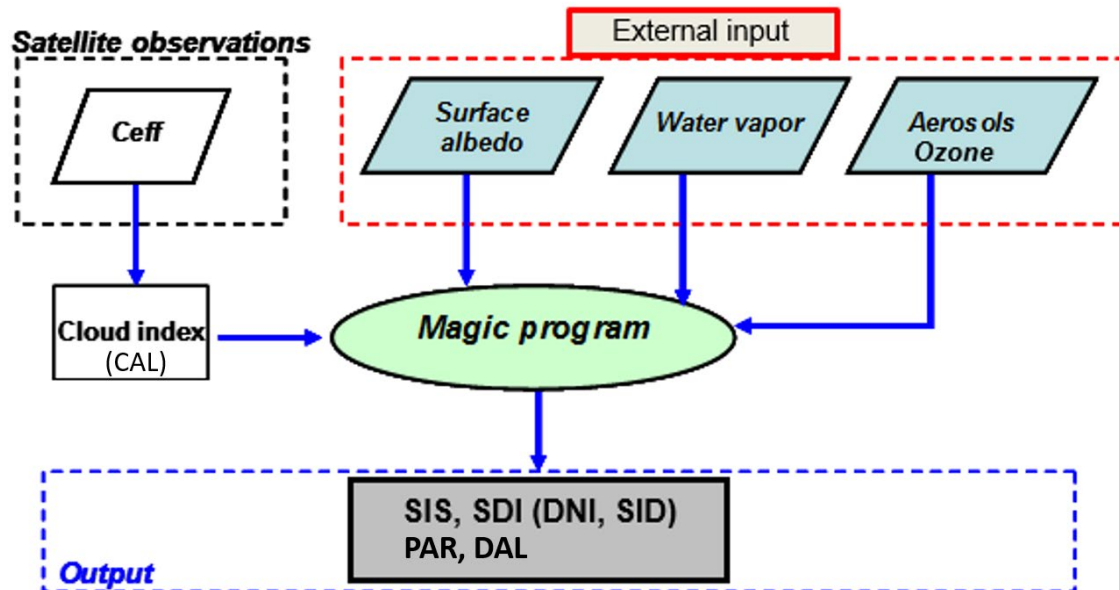


Figure 5-1: Diagram of the interface of gnu-MAGIC / SPECMAGIC to the atmospheric input and the satellite observations, Ceff stands for the dark offset corrected and normalised Counts.

5.1 Averaging

Daily averages of the surface solar radiation and the spectral radiation parameters are calculated from the instantaneous derived surface radiation parameters following the method published in Diekmann et al., 1988; (SIS is taken as example parameter):

Equation 5-1

$$SIS_{DA} = SIS_{CLSDA} \frac{\sum_{i=1}^n SIS_i}{\sum_{i=1}^n SIS_{CLS_i}}$$

SIS_{DA} is the daily average of SIS. SIS_{CLSDA} is the daily averaged clear sky SIS, SIS_i the calculated SIS for satellite image i and SIS_{CLS_i} the corresponding calculated clear sky SIS. The number of images available during a day is denoted by n .

The larger the number of available images per day, the better the daily cycle of cloud coverage can be resolved, increasing the accuracy of the daily average of SIS. Please note that the

	<p align="center">Algorithm Theoretical Basis Document SARAH-3</p>	<p>Doc. No: SAF/CM/DWD/ATBD/SARAH Issue: 3.5 Date: 24.02.2023</p>
---	---	---

diurnal cycle of the solar zenith angle is implicitly accounted for by using the clear sky daily mean SIS value in the averaging.

A minimum number of 25% available daylight pixels per day is required to derive the daily mean for the specific pixel. The monthly average of the radiation parameters is calculated following WMO criteria. That means a monthly mean cannot be calculated if more than ten daily values or five or more consecutive daily values are missing (WMO, 2018).

The conversion from the irregular satellite projection to the regular 0.05 x 0.05 degree regular lon-lat-grid is conducted with the gnu-MAGIC / SPECMAGIC gridding tool based on a nearest-neighbour method.

The temporal averaging of the SDI, i.e., the direct normalized surface solar radiation, DNI, and the direct surface solar radiation, SID, as well as of the spectral parameters PAR and DAL are conducted identical as for the surface solar irradiance, SIS, and are not repeated here.

5.2 Sensitivity and dependence on input parameters of SIS / SDI / PAR / DAL

The sensitivity of the surface solar radiation parameters on the input parameters is discussed. The section provides the uncertainty or sensitivity of the radiation parameters in relation to the input parameters. The error and accuracy of SIS is assessed by comparison with in-situ data and provided in the validation report. Beside the clear sky index, which is derived from satellite observations, aerosol and water vapour have a significant effect on the attenuation of the solar radiation parameters as well. A full uncertainty assessment can be found in RD 1, thus only the main results are summarized.

5.2.1 Water vapour


The sensitivity of the solar surface radiation on the integrated water vapour is higher for low water vapour amounts and low solar zenith angles. The total surface irradiance shows a stronger sensitivity to uncertainties in the integrated water vapour than the direct solar radiation. Overall uncertainties in the integrated water vapour of about 1 to 2 mm translate to uncertainties in surface irradiance of approx. 3 W/m², with slightly larger values under low water vapour conditions, and less uncertainty under high water vapour levels.

5.2.2 Ozone

The sensitivity of the solar surface radiation on the integrated ozone amount is in the order of 1 W/m² for typical ozone variation within the METEOSAT disk. Again, the sensitivity of the solar irradiance on ozone is slightly higher than that given for the direct irradiance.

5.2.3 Aerosols

The sensitivity of the surface solar radiation to uncertainties in aerosol information is mainly controlled by the aerosol optical depth (AOD). While the sensitivity of the direct irradiance by

	<p align="center">Algorithm Theoretical Basis Document SARAH-3</p>	<p>Doc. No: SAF/CM/DWD/ATBD/SARAH Issue: 3.5 Date: 24.02.2023</p>
---	---	---

aerosols is completely governed by the AOD, the total surface solar radiation is also sensitive to uncertainties in the aerosol type, expressed by the single scattering albedo and the asymmetry parameter. In all cases, the sensitivity does also depend on the solar zenith angle.

The sensitivity on uncertainties in the AOD is higher for the direct irradiance than for the global irradiance. Typical uncertainties in the monthly mean aerosol optical depth of 0.1 relative to a background of AOD=0.2 leads to uncertainties in SIS of about 10 W/m² for a solar zenith angle of 60 degree and about 20 W/m² for solar zenith angle of 0 degree, both assuming cloudless sky (values are approx. three times higher for SID). However, for cloudy conditions these uncertainties are reduced significantly with increasing cloud optical depth.

For the total surface solar radiation, additional uncertainties result from the assumptions on the aerosol optical properties, which can be in the same order of magnitude. Uncertain aerosol information are one of the major sources of the errors in the retrieval of surface solar radiation from satellite on short time scales. On the daily and monthly time scales, however, the aerosol impacts are substantially reduced compared to the instantaneous values. Further details are given in RD 1.

5.2.4 Surface albedo

The sensitivity of clear sky SIS on uncertainties and errors in the surface albedo is comparably small. Deviations of +/- 0.1 in the surface albedo lead to deviations in clear sky SIS of +/- 1%. The effect is almost linear. Errors in the surface albedo are expected to be typically less than 0.1, with higher deviation possible in case of snow covered surfaces. The effect is predominantly independent on the clear sky atmospheric state.

5.2.5 Clear sky index

The clear sky index is calculated from the effective cloud albedo (CAL) using Equation 3-10. For CAL>0.8 the clouds are optically rather thick and the uncertainty in the solar irradiance is small in absolute terms. Therefore, it is focused on the range between 0 and 0.8. Here any uncertainty in CAL leads to identical uncertainty in the clear sky index. As only the uncertainty arising from the cloud index is of interest, a small contribution of the clear sky irradiance to the overall uncertainty can be assumed.

As a result of the definition of the clear sky index, an uncertainty of x% translates directly in the identical relative uncertainty for the solar irradiance, meaning a 3 % uncertainty in the effective cloud albedo leads to a 3 % uncertainty in the solar irradiance.

For the direct surface solar radiation, the sensitivity on the clear sky index is larger. An uncertainty of 2% for the clear sky index results in an uncertainty of about 10 % in the direct irradiance, demonstrating the importance of an accurate clear sky index on the direct irradiance. Further information can be found in RD 1.

	<p style="text-align: center;">Algorithm Theoretical Basis Document SARAH-3</p>	<p>Doc. No: SAF/CM/DWD/ATBD/SARAH Issue: 3.5 Date: 24.02.2023</p>
---	--	---

5.3 Assumption, limitations and future improvements

- The strong clear sky reflection over bright surfaces (e.g., desert regions) reduces the contrast between clear sky reflection and cloudy-sky reflection. This leads to higher uncertainties in CAL and errors in the calculation of radiation parameters over bright surfaces.
- In regions with long-lasting cloud cover the used approach for the clear sky reflection overestimates the clear sky reflection. This results in an underestimation of the effective cloud albedo and an overestimation of the solar surface radiation.
- The accuracy of aerosol information is unknown in several regions of the world due to missing ground measurements. Any uncertainty in the aerosol information affects the accuracy of the surface solar radiation (in particular for the direct solar radiation), especially in regions that are dominated by clear sky.
- The use of a monthly climatology for the aerosol optical depth reduces the ability to correctly describe the effects of temporal changes in the aerosol concentration on the clear-sky and hence all-sky surface solar radiation.
- The quality of the direct irradiance strongly depends on the quality of the information about the atmospheric state, especially the aerosol information, the integrated water vapour and the clear sky index.
- The gnu-MAGIC / SPECMAGIC clear sky model does currently not explicitly consider topography for the clear sky surface radiation calculations. The integrated water vapour content is adjusted to account for its reduction at higher elevations; the impact of elevation on aerosol optical depth is considered on the coarse grid resolution. Only the effect of modified Rayleigh scattering is not accounted for, which is considered to be small.

	Algorithm Theoretical Basis Document SARAH-3	Doc. No: SAF/CM/DWD/ATBD/SARAH Issue: 3.5 Date: 24.02.2023
---	---	--

6 Spectral surface radiation parameters (PAR and DAL)

As SPECMAGIC internally is based on spectrally resolved radiation calculations, this feature can be used to derive radiation parameters covering a certain spectral range. Those dedicated spectral radiation parameters are for example the Photosynthetic Active Radiation (PAR), Daylight (DAL), or Ultra-violet radiation. The first two parameters mentioned are becoming official parameters in SARAH-3. The basic principle of retrieving those spectral parameters is to internally summing up and weighting of the relevant spectral bands.

In general, the retrieval is similar to retrieval of the broadband radiation parameters, using the same external input data and having similar dependencies and limitations.

The averaging of the spectral parameters is similar to the averaging of the broadband solar irradiance parameters. Assumptions and limitations described in section 5.3 are also valid for the spectral parameters.

6.1 Photosynthetic Active Radiation

Photosynthetic Active Radiation (PAR) is an important parameter in Biology and related fields (Asrar et. al 1992), and is defined as the part of the surface solar spectrum that can be used by plants to do photosynthesis. PAR is the surface solar radiation from 400 to 700 nm wavelengths (cf. Figure 6-1). Hence the affected spectral bands (so-called Kato-bands, Kato et al., 1999) are weighted and summed up to estimate PAR. The unit of the PAR data generated is $\mu\text{mol m}^{-2} \text{s}^{-1}$ – a commonly used unit for PAR in Biology and related fields. This unit can be transferred to W/m^2 by the approximation $1 \text{ W/m}^2 \approx 4.6 \mu\text{mole m}^{-2} \text{ s}^{-1}$ (Sager and Farlane, 2017).

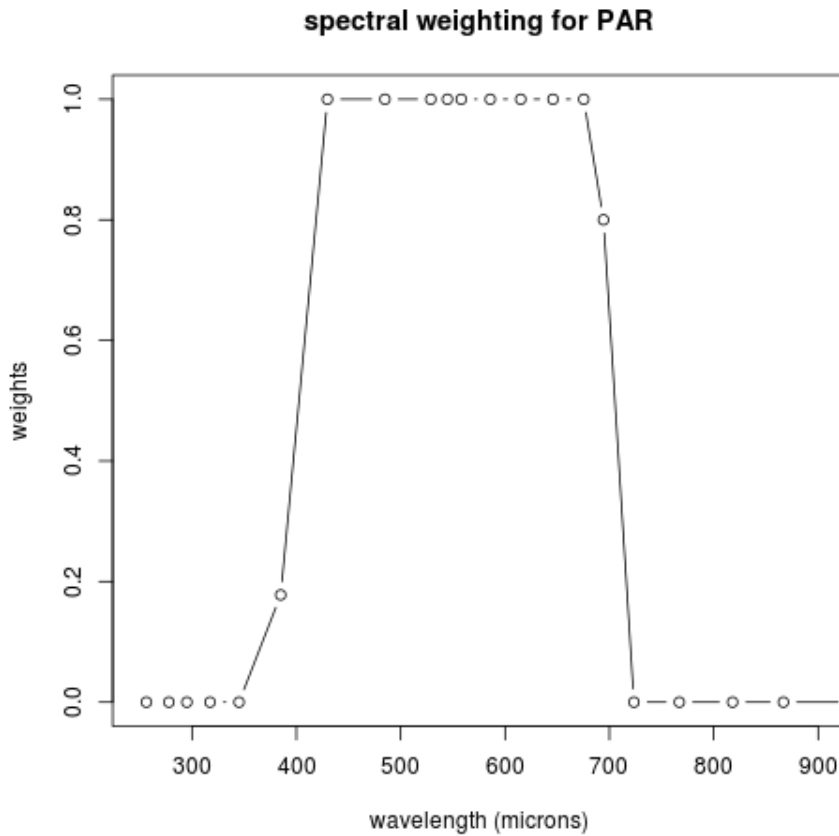


Figure 6-1: Spectral weighting of Kato-bands to generate PAR

6.2 Daylight (DAL)

Daylight (DAL) is defined as the intensity of light as observed by the human eye. Spectral weighting is shown in Figure 6-2. The unit of DAL is Lux, kilo-Lix (kLux) is used as the unit given in the DAL data record. As for PAR, DAL is generated by appropriate weighting and summing up of the relevant spectral bands. DAL is a relevant parameter for architectural applications. The unit Lux can be transferred to W/m^2 by the relation $1 \text{ kLux} \approx 1.46 \text{ W/m}^2$.

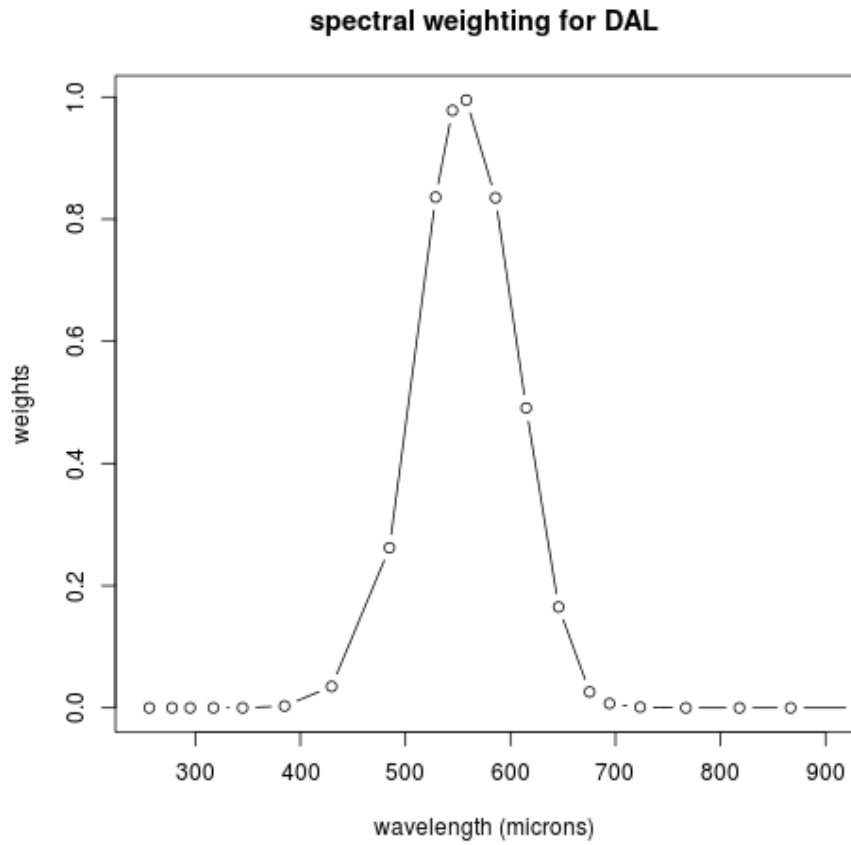


Figure 6-2: Spectral weighting of Kato-bands to generate DAL

7 Sunshine Duration

Basis for the retrieval of satellite-based sunshine duration (SDU) are the SARAH-3 DNI data and the WMO threshold for sunshine, which is defined by $DNI \geq 120 \text{ W/m}^2$ and a solar elevation angle exceeding 2.5° . SDU is derived by the ratio of sunny slots to all slots during daylight:

Equation 7-1 $SDU = \text{daylength} \times \frac{\sum_{i=1}^{\text{iday}} (W_i(\text{sunny slot}_i))}{\# \text{daylight slots}}$

The possible clear-sky daylength is pre-calculated depending on the date, longitude and latitude using the simplified SOLIS clear sky radiation model to estimate clear sky DNI (Ineichen, 2008, Antonanzas-Torres et al., 2019). Monthly climatological aerosol and water vapour information is used to include their effect on the DNI; the maximum possible daily sunshine duration is determined using a threshold of 2.5° for the solar elevation angle and of 120 W/m^2 for the DNI (Figure 7-1).

The W_i indicates a weighting of sunny slots depending on the number of surrounding cloudy and sunny grid points, which is discussed in more detail in section 4.1. The number of daylight slots ($\# \text{ daylight slots}$) describes the maximum number of Meteosat observations (slots) per grid point and per day during daylight as derived from clear sky estimations of DNI. Daily SDU is calculated only if 25% of the daylight slots are available.

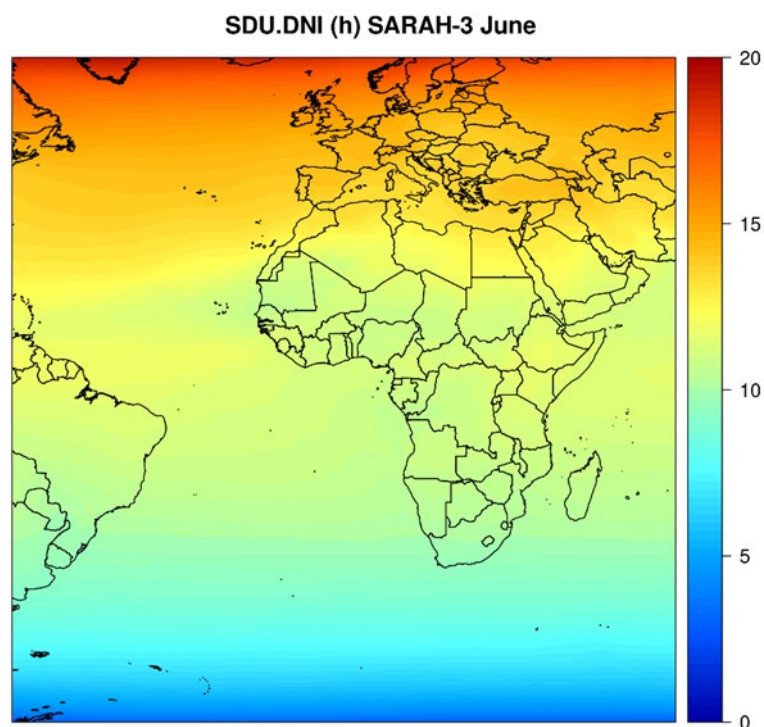


Figure 7-1: Clear sky daylength (h) based on $DNI \geq 120 \text{ W/m}^2$ for 1st of June.

7.1 Weighting of sunny slots

A sunny slot corresponds to a DNI value of 120 W/m² or larger. SARAH-3 provides instantaneous DNI data every 30 minutes. Therefore, without weighting, in Equation 7-1 one sunny slot would correspond to a 30 minutes time window. In reality this is only the case in bright weather situations. If there are clouds in the surrounding area of a grid point, there is a probability that not the whole 30 minutes are sunny. This is also valid in the opposite case, when a cloudy grid point has sunny grid points in its near surrounding's. This fact should be accounted for in the retrieval of SDU by using the information of the 24 surrounding grid points (see Figure 7-2).

In addition the information of two successive time steps is incorporated.

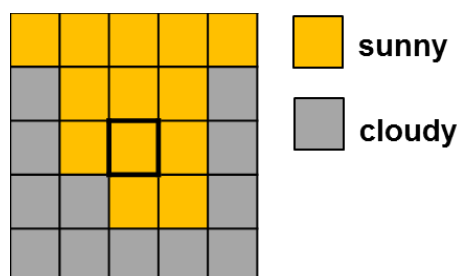


Figure 7-2: Demonstration for accounting for surrounding grid points. The target grid point is marked in the centre.

In a first step for each grid point the number of sunny grid points in an environment of 24 grid points is summed up. This is done for each daytime slot. The number of each time step is combined with the number of the previous time step to incorporate also the temporal movement of clouds in a simplified way (see Equation 7-2).

$$N_1 = \text{\#sunny area}_1 \times 0.04$$

Equation 7-2

$$N_i = (\text{\#sunny area}_i + \text{\#sunny area}_{i-1}) \times 0.02$$

The resulting number N is 1 in case that all grid points are sunny, and 0 in the case that no grid point is sunny.

In a second step the impact of cloudy and sunny grid points on the temporal length of one time slot is estimated. The grid points Sgp (sunny grid points) get the value 1 in case that DNI ≥ 120 W/m² and 0 in case DNI ≤ 120 W/m². The opposite is done for Cgp (cloudy grid points), where the grid point gets the value 1 in case that DNI ≤ 120 W/m² and 0 in case DNI ≥ 120 W/m². Two constant values were empirically determined to correct the influence of sunny or cloudy grid points.

Equation 7-3

$$\mathbf{Sgp}_i = \mathbf{Sgp}_i \times N_i \text{ with lower limit of } N_i \text{ is set to } C1$$

Equation 7-4

$$\mathbf{Cgp}_i = \mathbf{Cgp}_i \times (N_i \times C2)$$

	<p style="text-align: center;">Algorithm Theoretical Basis Document SARAH-3</p>	<p>Doc. No: SAF/CM/DWD/ATBD/SARAH Issue: 3.5 Date: 24.02.2023</p>
---	--	---

The sum of S_{gp} and C_{gp} is the fraction of the time, which one slot contributes to the sunshine duration of a slot.


Equation 7-5

$$W_i(\text{sunny slot}_i) = S_{gp_i} + C_{gp_i}$$

The final sunshine duration in hours is derived by Equation 7-1.

7.2 Assumption, limitations and future improvements

The constants C1 and C2 are empirical estimations, which were derived by simple test calculations using about 250 reference stations in Germany only. These tests have to be more systematic and for a larger and more representative number of reference stations. Another possible improvement can be done for the impact of the surrounding grid points. This influence is only estimated, as the real cloud motion is unknown by the retrieval algorithm. Using auxiliary input fields, such as cloud motion vectors, could further improve the sunshine duration.

	<p align="center">Algorithm Theoretical Basis Document SARAH-3</p>	<p>Doc. No: SAF/CM/DWD/ATBD/SARAH Issue: 3.5 Date: 24.02.2023</p>
---	---	---

8 Improvements relative to the released previous versions of the CM SAF Surface Radiation data records.

8.1 Improvements compared to the MVIRI Surface Radiation data record

The length of the data record has substantially been extended compared to the CM SAF MVIRI CDR.

Special care has been taken in order to improve the homogeneity of the CDR. The available CM SAF MVIRI CDR exhibits some breaks and inhomogeneities in Europe before 1994 (Sanchez-Lorenzo et al., 2013). There are also indications of artificial shifts in the data record in other regions (Brinckmann et al., 2013). Corrupted raw data are, at least partly, the source of these breaks and inhomogeneities. Due to problems with data transmission only every second line of the broadband visible channel had been transmitted during night and twilight hours. This has been considered within the processing of the first CM SAF MVIRI only data record (RD 1), according to the EUMETSAT documentation. However, much more hours and time periods are affected. For these times the lines have been incorrectly interpreted as defined due to a missing no-data value in the raw images. Moreover, many other images are corrupted without being documented or listed as such. The CM SAF team performed a visual inspection of the images in order to detect all corrupted or incomplete images. This visual inspection is very time consuming, but the only possibility to avoid the use of corrupted or incomplete images. Some flaws as missing or black lines can be treated by interpolation (see section 2.5) or by assigning non-defined values. However, many corrupted images cannot be used and have to be disregarded within the reprocessing in order to avoid corruption of the retrieved solar surface irradiance.

The transition between MFG and MSG is a source for serious breaks and inhomogeneities due to the change in the spectral observations from the MVIRI to the SEVIRI instruments. Respective issues have been investigated and resolved (Posselt et al. 2011; 2013). For the generation of the current SARAH data record an artificial visible broadband channel has been used.

The IDL interpolation routine leads to circle structures in the images and has been replaced by an algorithm of R. Müller, developed within gnu-MAGIC.

A bug in the routine for the calculation of the pixel scanning time has been fixed.

8.2 Improvements compared to the first version of SARAH data record (MVIRI/SEVIRI Ed.2)

The spectral-resolved surface solar radiation (SRI) and the sunshine duration (SDU) is provided as part of SARAH-V2 and its extension SARAH V2.1.

The length of the data record will be extended compared to the available CM SAF SARAH CDR.

	<p align="center">Algorithm Theoretical Basis Document SARAH-3</p>	<p>Doc. No: SAF/CM/DWD/ATBD/SARAH Issue: 3.5 Date: 24.02.2023</p>
---	---	---

Additional, special care has been taken in order to further improve the homogeneity of the CDR. In particular the SARAH V1 CDR has a tendency to provide lower values after 2006, indicating a possible inhomogeneity in the transition from the MVIRI to the SEVIRI instruments. The homogeneity of the MVIRI – SEVIRI transition has been improved compared to the SARAH V1 CDR. The application of SARAH-2.1 is demonstrated in climate studies (see e.g. Pfeifroth et al., 2018).

The geometric viewing angle effect on the cloud albedo has been considered using an empirical formula depending on the satellite zenith angle.

The integrated water vapour from ERA-Interim has been adjusted to include an elevation dependency. This does result in more realistic clear-sky surface radiation calculations, and, subsequently, has the largest impact on SIS and DNI in regions with high clear-sky contributions.

8.3 Improvements of SARAH-3 relative to the SARAH-2 data record (MVIRI/SEVIRI Ed.3)

The main innovation in the algorithm used to generate SARAH-3 is the estimation and the application of a daily snow mask using the Helsnow algorithm. By using the daily snow mask and its respective snow brightness, the estimation of surface solar radiation in case of snow-covered surfaces is substantially improved.

Further, the newly-implemented monthly surface albedo improves the calculation of the clear sky surface radiation retrieval over almost all land areas, with the largest changes being expected in desert regions. No / fewer missing data during sunrise and sunset will be present in the new SARAH-3 climate data record. In previous versions of SARAH a minimum sun elevation of $\sim 2.5^\circ$ was required to estimate surface radiation parameters. No threshold is used in the current processing.

The new atmospheric input from ERA5, which is used as daily data instead of monthly for its predecessor, is expected to overall improve the products in SARAH-3, especially the daily and sub-daily products.

The estimation of the sunshine duration benefits from the improvements in the surface radiation retrieval, in particular over snow-covered surfaces. The estimation of sunshine duration from the direct normal radiation (DNI) has been improved by considering the effect of the atmospheric aerosol on the local clear sky sunshine duration and the minimum solar zenith angle. In addition, the estimation of sunshine duration now ensures that the daily sunshine duration does not exceed the clear sky sunshine duration.

	<p align="center">Algorithm Theoretical Basis Document SARAH-3</p>	<p>Doc. No: SAF/CM/DWD/ATBD/SARAH Issue: 3.5 Date: 24.02.2023</p>
---	---	---

9 Adaptions for ICDR generation

The SARAH-3 retrieval algorithm requires some adaptions to be applicable for the generation of the SARAH-3 Interim Climate Data Record (ICDR). As the ICDR generates data in close to realtime, data from the ERA5 reanalysis are not available; also the approach to calculate each month separately and using their individual temporal statistics has to be adapted since one can only look backward in time. These adaptions result in small differences between the SARAH-3 CDR and the SARAH-3 ICDR. The validation of the ICDR data by comparison with the corresponding data from the CDR is presented in the SARAH-3 Validation Report.


9.1 Algorithmic adaptions

For the calculation of the daily snow mask (in the Helsnow module) the satellite data from the last 30 days (preceding the processed day) is used to derive the statistical information instead of the satellite data from the respective month (as in the CDR processing). The basic processing steps of Helsnow remain unchanged. Analogue to Helsnow, the last 30 days of data are also used in the Heliosat part for the retrieval of the Effective Cloud Albedo (CAL). Based on CAL, Spcsmagic calculates the 30-min and daily-averaged surface radiation parameters the same way as in the CDR processing; also the monthly means are calculated from the daily averaged data using WMO criteria.

9.2 Auxiliary data


For the ICDR generation near-realtime auxiliary data of water vapour, ozone, snow and sea-ice is required which can not be gathered from ERA5. Data from the ECMWF operation high-resolution analysis (snow and sea-ice) and forecasts (water vapour, ozone) is used instead. This data has a higher spatial resolution (0.1x0.1 degree) than ERA5. Hence downscaling of the total column water vapour is not necessary and not applied in the ICDR processing.

In detail, for total column water vapour and total column ozone the time steps 0 UTC (analysis), 6 UTC (0+6h-forecast), 12 UTC (analysis), 18 UTC (12+6h-forecast) are used to calculate daily means, which are used in the retrieval. For snow depth and sea-ice thickness the 12 UTC analysis is used. The data is collected as quick as possible from the ECMWF database in order to allow a timely start of the processing.

	Algorithm Theoretical Basis Document SARAH-3	Doc. No: SAF/CM/DWD/ATBD/SARAH Issue: 3.5 Date: 24.02.2023
---	---	--

10 References

- Antonanzas-Torres, F., R. Urraca, J. Polo, O. Perpiñán-Lamigueiro, R. Escobar, 2019: Clear sky solar irradiance models: A review of seventy models, *Renewable and Sustainable Energy Reviews*, 107, 374 – 387.
- Asrar G., Myneni, R.B., Choudhury, B.J., 1992: Spatial heterogeneity in vegetation canopies and remote sensing of absorbed photosynthetically active radiation: A modeling study, *Remote Sensing of Environment*, 41, 85-103.
- Bellouin, N., Quaas, J., Morcrette, and J.-J., Boucher, O., 2013: Estimates of aerosol radiative forcing from the MACC re-analysis, *Atmos. Chem. Phys.*, 13, 2045-2062.
- Benedetti, A., Morcrette, J.-J., Boucher, O., Dethof, A., Engelen, R.J., Fisher, M., Flentje, H., Huneus, N., Jones, L., Kaiser, J.W., Kinne, S., Mangold, A., Razinger, M., Simmons, A.J., Suttie, M., Aerosol analysis and forecast in the European Centre for Medium-Range Weather Forecasts Integrated Forecast System: 2. Data assimilation, *J. Geophys. Res.*, 2009, 114, D13205
- Bento, V., 2016: Improving Land Surface Temperature retrievals over mountainous regions, Poster presented at the DUE GlobTemperature User Consultation Meeting #4, Lisbon, June 2016.
- Beyer, H. G., C. Costanzo, and D. Heinemann, 1996: Modifications of the Heliosat procedure for irradiance estimates from satellite images. *Solar Energy*, 56, 207-212.
- Blanc P., Gschwind, B., Ménard, L., Wald, L., 2018: Monthly-averaged maps of surface BRDF parameters in ten spectral bands for land and water masses. *Earth Syst. Sci. Data Discuss.*, <https://doi.org/10.5194/essd-2017-141>.
- Brinckmann S, Trentmann J, Ahrens B. Homogeneity Analysis of the CM SAF Surface Solar Irradiance Dataset Derived from Geostationary Satellite Observations. *Remote Sensing*. 2014; 6(1):352-378.
- Cano, D., J. M. Monget, M. Albuissou, H. Guillard, N. Regas, and L. Wald, 1986: A method for the determination of the global solar-radiation from meteorological satellite data. *Solar Energy*, 37, 31-39.
- Copernicus Climate Change Service (C3S) (2017): ERA5: Fifth generation of ECMWF atmospheric reanalyses of the global climate . Copernicus Climate Change Service Climate Data Store (CDS), autumn 2019. <https://cds.climate.copernicus.eu/cdsapp#!/home>
- Cros, S.; Albuissou, M.; Wald, L., Simulating Meteosat-7 broadband radiances using two visible channels of Meteosat-8. *Solar Energy*, 2006, 80, 361–367.
- Dagestad, K.-F. Mean bias deviation of the Heliosat algorithm for varying cloud properties and sun-ground-satellite geometry, *Theor. Appl. Climatol.*, 2004, 79, 215–224, DOI 10.1007/s00704-004-0072-5

	Algorithm Theoretical Basis Document SARAH-3	Doc. No: SAF/CM/DWD/ATBD/SARAH Issue: 3.5 Date: 24.02.2023
---	---	--

Dee, D., et al., The ERA-Interim reanalysis: configuration and performance of the data assimilation system, *Q. J. R. Meteorol. Soc.*, 2011, 137: 553–597.

Diekmann, F.J., S. Happ, M. Rieland, W. Benesch, G. Czeplak, F. Kasten, An operational estimate of global solar irradiance at ground level from METEOSAT data: results from 1985 to 1987, 1988, *Meteorol. Rdsch.*, 41, 65-79.

Dürr, B., and A. Zelenka, 2009: Deriving surface global irradiance over the Alpine region from METEOSAT Second Generation data by supplementing the HELIOSAT method. *International Journal of Remote Sensing*, 5821-5841.

Farnebäck G.: Two-Frame Motion Estimation Based on Polynomial Expansion. In: Bigun J, Gustavsson T, editors. *Image Analysis*. Springer Berlin Heidelberg; 2003. pp. 363–370. doi:10.1007/3-540-45103-X_50

Hammer, A., D. Heinemann, C. Hoyer, R. Kuhlemann, E. Lorenz, I. Müller, R., and H. G. Beyer, 2003: Solar energy assessment using remote sensing technologies. *Remote Sens. Environ.*, 86, 423--432.

Hammer, A., 2000. *Anwendungsspezifische Solarstrahlungsinformationen aus Meteosat-Daten*. Phd, School of Mathematics and Natural Sciences, University of Oldenburg.

Hersbach, H, Bell, B, Berrisford, P, et al. The ERA5 global reanalysis. *Q J R Meteorol Soc.* 2020, 146: 1999– 2049. <https://doi.org/10.1002/qj.3803>

Hess, M.; P. Köpke; I. Schult: *Optical Properties of Aerosols and Clouds: The Software Package OPAC*. *Bull. Amer. Meteor. Soc.*, 1998, 79, 831-844.

Ineichen, P.: A broadband simplified version of the Solis clear sky model, *Solar Energy*, 2008, 82, 758-762.

Kato, S., Ackerman, T., Mather, J., and Clothiaux, E.: The k-distribution method and correlated-k approximation for short-wave radiative transfer model, *J. Quant. Spectrosc. Ra.* 1999, 62, 109–121.


Kinne, S., Schulz M., Textor C. et al. : An AeroCom initial assessment – optical properties in aerosol component modules of global models, *Atmos. Chem. Phys.*, 2006, 6, 1815-1834.

Köpke P.; Hess M.; Schult I.; Shettle E., *Global aerosol data set*. Tech. Rep., 1887, 243, MPI Meteorology, Hamburg.

Kothe, S., Good, E. Obregón, A. Ahrens, B., Nitsche, H.: *Satellite-Based Sunshine Duration for Europe*. *Remote Sens.* 2013, 5(6), 2943-2972; doi:10.3390/rs5062943

Mayer B.; A. Kylling, Technical note: “The libRadtran software package for radiative transfer calculations - description and examples of use.” *Atmos. Chem. Phys.*, 2005, 5, 1855-1877.

Morcrette, J. J., Boucher, O., Jones, L., Salmond, D., Bechtold, P., Beljaars, A., Benedetti, A., Bonet, A., Kaiser, J. W., Razinger, M., Schulz, M., Serrar, S., Simmons, A. J., Sofiev, M., Suttie, M., Tompkins, A. M., Untch, A., *Aerosol analysis and forecast in the European Centre for*

	Algorithm Theoretical Basis Document SARAH-3	Doc. No: SAF/CM/DWD/ATBD/SARAH Issue: 3.5 Date: 24.02.2023
---	---	--

Medium-Range Weather Forecasts Integrated Forecast System: Forward modelling, J. Geophys. Res., 2009, 114

Müller, R.W. et al., Report of the HELIOSAT-3 software package for solar irradiance retrieval, all sky working version" EU report of the Heliosat-3 project (www.heliosat3.de), NNE5-2000-00413, 2003

Mueller, R., U. Pfeifroth, and C. Traeger-Chatterjee, 2015: Towards Optimal Aerosol Information for the Retrieval of Solar Surface Radiation Using Heliosat. Atmosphere, 6, 863-878.

Mueller, R.W., K.F. Dagestad, P. Ineichen, M. Schroedter-Homscheidt, S. Cros, D. Dumortier, R., Kuhlemann R. ; Olseth J.A.; Piernavieja G.; Reise C.; Wald L.; Heinemann D.; Rethinking satellite based solar irradiance modelling – The SOLIS clear sky module", Rem. Sens. Envir., 2004, 91, 160-174.

Mueller, R., C. Matsoukas, A. Gratzki, H. Behr, and R. Hollmann, 2009: The CM-SAF operational scheme for the satellite based retrieval of solar surface irradiance - A LUT based eigenvector hybrid approach. Remote Sensing of Environment, 1012-1024.

Mueller, R., T. Behrendt, A. Hammer, and A. Kemper, 2012: A New Algorithm for the Satellite-Based Retrieval of Solar Surface Irradiance in Spectral Bands. Remote Sensing, 4, 622-647.

Mueller, R., and C. Träger-Chatterjee, 2014: Brief Accuracy Assessment of Aerosol Climatologies for the Retrieval of Solar Surface Radiation. Atmosphere, 5, 959-972.

Müller, R., U. Pfeifroth, C. Träger-Chatterjee, J. Trentmann, and R. Cremer, 2015: Digging the METEOSAT Treasure—3 Decades of Solar Surface Radiation. Remote Sensing, 7, 8067-8101.

Muñoz-Sabater, J., Dutra, E., Agustí-Panareda, A., Albergel, C., Arduini, G., Balsamo, G., Boussetta, S., Choulga, M., Harrigan, S., Hersbach, H., Martens, B., Miralles, D. G., Piles, M., Rodríguez-Fernández, N. J., Zsoter, E., Buontempo, C., and Thépaut, J.-N.: ERA5-Land: A state-of-the-art global reanalysis dataset for land applications, Earth Syst. Sci. Data, 13, 4349–4383, 2021. <https://doi.org/10.5194/essd-13-4349-2021>.

Perez, R., Seals, R., Zelenka, A., Production of Site/Time-specific Hourly Irradiances -Satellite Remote Sensing vs. Network Interpolation, in Production of Site/Time-specific Irradiances from Satellite and Ground Data, published by New York State Energy Research and Development Authority , 1998, Report 98-3.

Perez, R. et al., 2001, Solar resource assessment: A review, in Solar Energy - The state of the art, published by James & James Science Publishers, 497-562.

Pfeifroth, U., Sanchez-Lorenzo, A., Manara, V., Trentmann, J., & Hollmann, R. (2018). Trends and variability of surface solar radiation in Europe based on surface- and satellite-based data records. Journal of Geophysical Research: Atmospheres, 123, 1735– 1754. <https://doi.org/10.1002/2017JD027418>

	Algorithm Theoretical Basis Document SARAH-3	Doc. No: SAF/CM/DWD/ATBD/SARAH Issue: 3.5 Date: 24.02.2023
---	---	--

Posselt R, Mueller R, Stöckli R, Trentmann J. Spatial and Temporal Homogeneity of Solar Surface Irradiance across Satellite Generations. *Remote Sensing*. 2011; 3(5):1029-1046.

Posselt R., Müller, R.W., Stöckli R., Trentmann, J., 2012, Remote sensing of solar surface radiation for climate monitoring - the CM-SAF retrieval in international comparison, *Remote Sens. Environ.*, 118, 186-198, doi: 10.1016/j.rse.2011.11.

Posselt, R., Mueller R., Trentmann J., Stoeckli R., Liniger M., Extension of the CM SAF surface radiation climatology (MAGIC SOL) beyond Meteosat First Generation Satellites, accepted for publication in *Remote Sensing of Environment*, 2013.

Rigollier C., Lefevre M., Blanc P., and Wald L.: The operational calibration of images taken in the visible channel of the meteosat series of satellites, *J. Atmos. Ocean. Technol.*, 2002, 19, 1285-1293.

Rigollier C., Lefevre M., and Wald L., 2004: The method Heliosat-2 for deriving shortwave solar radiation from satellite images, *Solar Energy*, 77, 159–169.

Sager, J. C. and Mc Farlane, J. C., 2017: Chapter 1: Radiation, *Plant Growth Chamber Handbook*, North Central Regional Research Publications No. 340, Iowa Agriculture and Home Economics Experiments Station Special Report No. 99.
<https://www.controlledenvironments.org/wp-content/uploads/sites/6/2017/06/Ch01.pdf>

Sanchez-Lorenzo, A., Wild, A.M., Trentmann, J., 2013. Validation and stability assessment of the monthly mean CM SAF surface solar radiation dataset over Europe against a homogenized surface dataset (1983–2005), *Remote Sens. Environ.*, 134, 355-366, doi: 10.1016/j.rse.2011.11. doi: 10.1016/j.rse.2013.03.012

Skartveit A., Olseth J., Tuft M., 1998: An hourly diffuse fraction model with correction for variability and surface albedo. *Solar Energy*, 63, 173–183.

Wald, L..et al., SoDa: A project for the integration and exploitation of networked solar radiation databases, in *Environmental Communication in the Information Society*, Published by the International Society for Environmental Protection, Vienna, Austria, Editors: Pillmann and Tochtermann, 2002, 713-720.

WMO-No. 100, Guide to Climatological Practices, 2018 edition, 2018.

Zelenka, A., R. Perez, R. Seals, D. Renne, 1999: Effective Accuracy of Satellite-Derived Hourly Irradiances, *Theor. Appl. Climatol.*, 62, 199 – 207.

11 Glossary – List of Acronyms

AOD	Aerosol Optical Depth
CAL	Effective Cloud Albedo
CDOP	Continuous Development and Operational Phase
CDR	Climate Data Record
CM SAF	Satellite Application Facility on Climate Monitoring
DAL	Daylight
DWD	Deutscher Wetterdienst
DNI	Direct Normal Irradiance
ECMWF	European Centre for Medium-Range Weather Forecast
ECV	Essential Climate Variable
ERA	ECMWF Reanalysis
GADS/OPAC	Global Aerosol Data Set / Optical Properties of Aerosols and Clouds
GCOS	Global Climate Observing System
GERB	Geostationary Earth Radiation Experiment
ICDR	Interim Climate Data Record
K	Clear sky index
LUT	RTM based Look-Up-Table
MAD	Mean of absolute deviation over several days or months
MVIRI	Meteosat Visible-InfraRed Imager
MACC	Monitoring Atmospheric Composition and Climate
PAR	Photosynthetic Active Radiation
RD	Reference Document
RTM	Radiative Transfer Model
SARAH	Surface Solar Radiation Data records – Heliosat
SDI	Surface Direct Irradiance (consist of SID and DNI)
SDU	Sunshine Duration

SEA	Sun Elevation Angle
SEVIRI	Spinning Enhanced Visible and InfraRed Imager
SID	Surface Incoming Direct radiation, commonly called direct irradiance
SIS	Surface Incoming Solar radiation, commonly called global irradiance or surface solar irradiance
SRI	Spectral Resolved Irradiance
SSA	Single Scattering Albedo
SZA	Solar Zenith Angle